

Long Range Interactions in Cosmology: Implications for Neutrinos

Ivan Esteban ^{a,b,c} Jordi Salvado ^c

^aCenter for Cosmology and AstroParticle Physics (CCAPP), Ohio State University, Columbus, OH 43210

^bDepartment of Physics, Ohio State University, Columbus, OH 43210

^cDepartament de Física Quàntica i Astrofísica and Institut de Ciències del Cosmos, Universitat de Barcelona, Diagonal 647, E-08028 Barcelona, Spain

E-mail: esteban.6@osu.edu, jsalvado@icc.ub.edu

Abstract. Cosmology is well suited to study the effects of long range interactions due to the large densities in the early Universe. In this article, we explore how the energy density and equation of state of a fermion system diverge from the commonly assumed ideal gas form under the presence of scalar long range interactions with a range much smaller than cosmological scales. In this scenario, “small”-scale physics can impact our largest-scale observations. As a benchmark, we apply the formalism to self-interacting neutrinos, performing an analysis to present and future cosmological data. Our results show that the current cosmological neutrino mass bound is fully avoided in the presence of a long range interaction, opening the possibility for a laboratory neutrino mass detection in the near future. We also demonstrate an interesting complementarity between neutrino laboratory experiments and the future EUCLID survey.

Contents

1	Introduction	1
2	Formalism	2
2.1	Homogeneous and Isotropic Scenario	4
2.1.1	Evolution Equations	4
2.1.2	Solution for a Thermal Fermion Relic	6
2.2	Perturbations and Instability	9
3	Cosmological Observables and Data Analysis: Neutrinos as a Benchmark	12
3.1	Analysis of Present Data	13
3.2	Future Prospects for Large Scale Structure	18
4	Summary and Conclusions	21
A	Classical Limit of the Evolution Equations	24
B	Properties of the Adiabatic Instability	25
C	Statistical Analysis in the Whole Parameter Space	28

1 Introduction

The quest for exploring new fundamental interactions has traditionally focused on high-energy probes such as particle colliders. The main hypothesis underlying these searches is that new physics has evaded detection because it only acts at short distances or, in particle physics terms, is mediated by heavy states. However, new physics could be mediated by light particles (i.e., it could have a long range) and remain undiscovered simply because it couples too weakly to matter.

In this case, small couplings can be overcome by setups with large amounts of particles over which effects accumulate coherently [1–5]. An archetypal example is gravity: despite being exceptionally weak, it was the first fundamental force discovered as it adds up over all particles in macroscopic objects. Cosmology is particularly well suited to explore this sort of many-particle effects, as in the early Universe particle number densities were extraordinarily high — at Big Bang Nucleosynthesis, for instance, as large as $\mathcal{O}(\text{MeV}^3) \sim 10^{32} \text{ cm}^{-3}$. Furthermore, cosmological evolution is dominated by gravity, and it is thus susceptible to be modified by any stronger interaction.

Along this line, long range interactions would directly impact cosmological structure formation, a hypothesis that has been widely explored in modified gravity and fifth force scenarios [6–22]. But cosmology is also sensitive to the total energy density and pressure of the Universe. These are commonly computed assuming that the homogeneous and isotropic cosmological fluid behaves as an ideal gas. Nevertheless, this assumption breaks down under the presence of an interaction whose range is larger than the interparticle distance. In this work, we will consistently study such effects and their observable consequences in cosmology. We will focus on interactions among fermions mediated by scalar fields, as they are simple

and universally attractive. That is, their effects accumulate over all particles and antiparticles with any spin orientation.

On top of that, we will face these models with the current precise cosmological data. To this purpose, we will focus on long range interactions among neutrinos. These particles are abundantly produced in the early Universe, significantly affecting its evolution, but their self interactions are poorly constrained [23–29]. The cosmological impact of putative neutrino self interactions has been widely studied [30–36], and lately there has been a renewed interest due to their possible relationship to the Hubble tension [37–46] or the short baseline neutrino anomalies [45–53]. The interactions explored in the literature are generically mediated by heavy particles, but if the mediator is light long range effects need to be taken into account. And, in fact, electroweak gauge invariance along with the absence of new physics in the charged lepton sector suggests that new neutrino interactions should be mediated by light particles [25, 54–56].

The study of neutrino properties is also an interesting topic by itself, as the observation of mass-induced neutrino flavour transitions constitutes our first laboratory evidence for physics beyond the Standard Model [57–59]. In particular, measuring the absolute neutrino mass scale is the holy grail of neutrino physics, as it would be a hint towards a new energy scale of Nature. Cosmology is particularly appropriate for this purpose, because massive neutrinos should become non-relativistic at times in which they impact Cosmic Microwave Background (CMB) and Large Scale Structure (LSS) data. Future surveys aim to pin down the absolute neutrino mass scale at the $\gtrsim 3\sigma$ level [60–63], much more precisely than current and near future laboratory experiments [64–68]. Relaxing the cosmological neutrino mass bound has been a subject of intensive research [69–77], particularly because if taken at face value the current bound from CMB data [78] implies that the neutrino mass scale is beyond the reach of present and near future laboratory experiments. As we will see, neutrino long range interactions drastically affect this bound.

This article is structured as follows. In Section 2 we introduce our formalism for a generic self-interacting fermion. We study and numerically solve the equations of motion for the homogeneous and isotropic case in Section 2.1, and in Section 2.2 we consider linear perturbations and their stability. In Section 3 we focus on neutrino long range interactions, showing their impact on current cosmological data (Section 3.1) as well as the future prospects with the LSS EUCLID survey (Section 3.2). We summarize our results and conclude in Section 4.

2 Formalism

As discussed in the Introduction, we will study scalar-mediated long range interactions among fermions. The action of the system is given by¹

$$S = \int \sqrt{-\mathcal{G}} d^4x \left(-\frac{1}{2} D_\mu \hat{\phi} D^\mu \hat{\phi} - \frac{1}{2} M_\phi^2 \hat{\phi}^2 + i \bar{\psi} \not{D} \psi - m_0 \bar{\psi} \psi - g \hat{\phi} \bar{\psi} \psi \right), \quad (2.1)$$

where $\hat{\phi}$ and ψ are the scalar and fermion fields respectively, \mathcal{G} is the determinant of the metric and D_μ its associated covariant derivative, M_ϕ and m_0 are the scalar and fermion

¹The formalism is similar to that of models where dark energy is induced by neutrinos or dark matter [7, 79–83]. Nevertheless, in those models the scalar field has a more exotic potential to mimic dark energy. Because of this, our scenario has different physical consequences.

masses respectively, g is the interaction coupling, and we have used the metric signature $(-, +, +, +)$. The equations of motion immediately follow

$$-D_\mu D^\mu \hat{\phi} + M_\phi^2 \hat{\phi} = -g \bar{\psi} \psi, \quad (2.2)$$

$$i \not{D} \psi - (m_0 + g \hat{\phi}) \psi = 0. \quad (2.3)$$

Equations (2.2) and (2.3) are equations for the quantum fields $\hat{\phi}$ and ψ . However, as we are interested in studying cosmological scales, the coherence length of the fermion field is generically much smaller than any considered distance. Thus, it can be analyzed in terms of a phase space distribution $f(x^\mu, P_\mu)$ of classical particles with positions x^μ and conjugate momenta P_μ . Analogously, the sourced scalar field will generically have a large occupation number, and can be well described by a classical field $\phi(x^\mu)$.

In this limit (see Appendix A for the details), the Dirac-like equation (2.3) gives the dispersion relation for the fermions

$$P_\mu P^\mu = -\tilde{m}^2, \quad (2.4)$$

where

$$\tilde{m} \equiv m_0 + g\phi \quad (2.5)$$

is the effective fermion mass. The classical limit of Eq. (2.2) reads (see Appendix A)

$$-D_\mu D^\mu \phi + M_\phi^2 \phi = -g \int \frac{dP_1 dP_2 dP_3}{\sqrt{-\mathcal{G}}} \frac{\tilde{m}}{P^0} f(x^\mu, P_\mu), \quad (2.6)$$

where the right hand side corresponds to the expectation value of $\bar{\psi} \psi$ evaluated for the fermion state. If the space-time components of the metric vanish, we can rewrite Eq. (2.6) in terms of the physical momentum \vec{p} as

$$-D_\mu D^\mu \phi + M_\phi^2 \phi = -g \int d^3 \vec{p} \frac{m_0 + g\phi}{\sqrt{|\vec{p}|^2 + (m_0 + g\phi)^2}} f(x^\mu, P_\mu(\vec{p})). \quad (2.7)$$

Both particles and antiparticles, with any spin orientation, equally contribute to f .

Equation (2.7) shows that the sourced scalar field ϕ is generically suppressed in two scenarios:

1. $|\vec{p}| \gg m_0$,² i.e., for ultrarelativistic fermions.
2. $\int f d^3 \vec{p} \ll M_\phi^3$, i.e., for number densities much smaller than the inverse interaction volume.

This is illustrated in Fig. 1, where we illustrate in blue the scalar field sourced by fermions (purple dots) with a characteristic energy T and number density n .

The fermion distribution function $f(x^\mu, P_\mu)$ evolves according to the Boltzmann equation [84]

$$\frac{\partial f}{\partial x^0} + \frac{dx^i}{dx^0} \frac{\partial f}{\partial x^i} + \frac{dP_i}{dx^0} \frac{\partial f}{\partial P_i} = \left(\frac{\partial f}{\partial x^0} \right)_C, \quad (2.8)$$

²As we will see in Section 2.1.1, for stationary solutions $-m_0 \leq g\phi \leq 0$. Thus, $|\vec{p}| \gg m_0$ also implies $|\vec{p}| \gg m_0 + g\phi$.

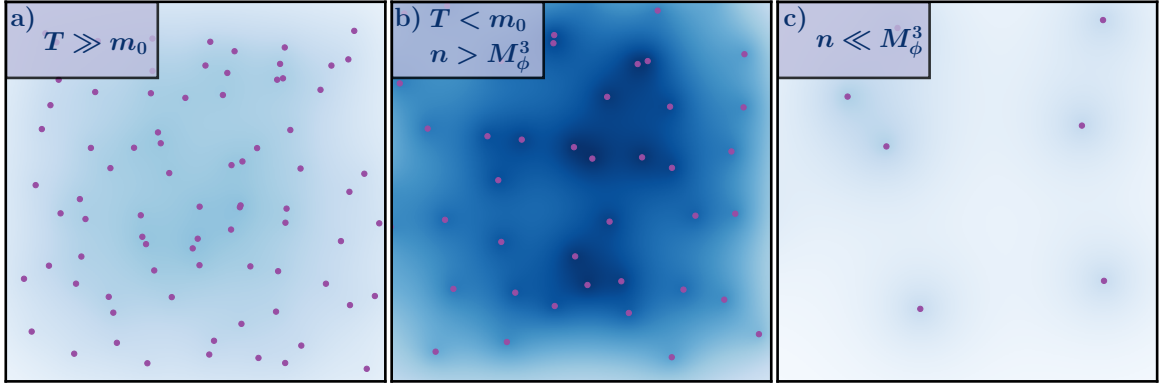


Figure 1: Illustration of the three relevant physical regimes for a system of massive fermions [purple dots] with a long range interaction mediated by a scalar field [blue]. T and n are the characteristic fermion kinetic energy and number density, respectively. For ultrarelativistic fermions, in panel (a); and interparticle distances above the interaction range $\sim M_\phi^{-1}$, in panel (c); there are no long range effects.

where the right hand side is the collision term, $\frac{dx^i}{dx^0} = \frac{P^i}{P^0}$ [84], and $\frac{dP_i}{dx^0}$ can be obtained from the geodesic equation of a fermion coupled with an external scalar field [85, 86]

$$P^0 \frac{dP^\mu}{dx^0} + \Gamma_{\alpha\beta}^\mu P^\alpha P^\beta = -\tilde{m}g\partial^\mu\phi, \quad (2.9)$$

where $\Gamma_{\alpha\beta}^\mu$ are the Christoffel symbols.

2.1 Homogeneous and Isotropic Scenario

2.1.1 Evolution Equations

Equations (2.7) to (2.9) fully characterize the evolution of the system. In this Section, we will solve them for a spatially flat homogeneous and isotropic Universe, described by the FLRW metric [87–90]

$$ds^2 = a(\tau)^2 (-d\tau^2 + \delta_{ij}dx^i dx^j), \quad (2.10)$$

where a is the scale factor, and $\tau \equiv \int \frac{dt}{a}$ is the conformal time with t the cosmological time. The evolution of the scale factor is related to the total energy density of the Universe ρ_{tot} through the Friedman equation

$$\left(\frac{da}{d\tau}\right)^2 = \frac{8\pi G_N}{3} a(\tau)^4 \rho_{\text{tot}}, \quad (2.11)$$

with G_N the Newton gravitational constant.

In a homogeneous and isotropic Universe, the fermion distribution function $f(x^\mu, P_\mu)$ can only depend on τ and the modulus of the momentum:

$$f(x^\mu, P_\mu) = f_0(\tau, q), \quad (2.12)$$

where $q \equiv a|\vec{p}|$. The Boltzmann equation then reads

$$\frac{\partial f_0}{\partial \tau} + \frac{dq}{d\tau} \frac{\partial f_0}{\partial q} = \left(\frac{\partial f_0}{\partial \tau}\right)_C. \quad (2.13)$$

$\frac{dq}{d\tau}$ can be obtained from the 0th component of the geodesic equation (2.9). After some algebra, we obtain

$$\frac{dq}{d\tau} = 0. \quad (2.14)$$

As discussed in the Introduction, we are interested in studying long range interaction effects. To isolate them, we will not include the collision term in the Boltzmann equation (2.12).³ Physically, this would correspond to small coupling constants g . As we will see, long range effects can still be relevant since they scale as $\frac{g}{M_\phi}$. Under this hypothesis, Eq. (2.12) reads

$$\frac{\partial f_0(\tau, q)}{\partial \tau} = 0. \quad (2.15)$$

That is, *any homogeneous and isotropic fermion distribution function that depends only on the combination $q = a|\vec{p}|$ does not evolve with time even under the presence of a long range scalar interaction.*

The equation of motion (2.7) for a homogeneous scalar field $\phi_0(\tau)$ reads

$$\frac{\phi_0''}{a^2} + 2H \frac{\phi_0'}{a} + M_\phi^2 \phi_0 = -g \int d^3\vec{p} \frac{m_0 + g\phi_0}{\sqrt{|\vec{p}|^2 + (m_0 + g\phi_0)^2}} f_0(\tau, a|\vec{p}|), \quad (2.16)$$

where primes denote derivatives with respect to conformal time and $H \equiv \frac{1}{a} \frac{da}{dt} = \frac{a'}{a^2}$ is the Hubble parameter. That is, we obtain a Klein-Gordon equation with a field-dependent source term, which will induce an effective scalar mass

$$M_T^2 \equiv \frac{\partial}{\partial \phi_0} \left(g \int d^3\vec{p} \frac{m_0 + g\phi_0}{\sqrt{|\vec{p}|^2 + (m_0 + g\phi_0)^2}} f_0(\tau, a|\vec{p}|) \right). \quad (2.17)$$

In Eq. (2.16), there are two characteristic timescales: on the one hand, H^{-1} , which controls both the Hubble friction term $2H \frac{\phi_0'}{a}$ as well as the rate at which the right-hand side changes.⁴ On the other hand, the inverse scalar field mass

$$M_{\text{eff}}^{-1} \equiv (M_\phi^2 + M_T^2)^{-1/2}, \quad (2.18)$$

which controls its characteristic oscillation time. Depending on the relative values of these timescales, we can distinguish three qualitatively different scenarios:

- $M_{\text{eff}} \ll H$ for all relevant times. In this case, $\phi_0(\tau)$ would be frozen to its value after inflation, and the physics of the scalar field would be that of quintessence, widely studied in the literature [91–98]. Furthermore, the scalar field sourced by the fermion background (that is, the right-hand side in Eq. (2.16)) would play no significant role. Since we are interested in the effect of fermion self interactions, we will not consider this scenario in this work.
- $M_{\text{eff}} \sim H$. In this case, $\phi_0(\tau)$ is determined by a non-trivial interplay among its initial condition and the fermion background. As we only want to study the effect of the latter, we will not consider this scenario in this work.

³Notice that, if collisions are relevant, one may also have to consider ϕ particle production and fermion-antifermion annihilation.

⁴Because of Eq. (2.15), $f_0(\tau, a|\vec{p}|)$ only depends on time through the scale factor in the second argument.

- $M_{\text{eff}} \gg H$ for all relevant times. As we will see next, in this case the physics of a fermion background interacting with a scalar field is insensitive to the initial condition of the latter. This will be the scenario studied in this work.

We can study the $M_{\text{eff}} \gg H$ scenario by using the adiabatic approximation. This corresponds to writing $\phi_0(\tau) = \overline{\phi}_0(\tau) + \varphi(\tau)$, where $\overline{\phi}_0$ satisfies

$$M_\phi^2 \overline{\phi}_0 \equiv -g \int d^3\vec{p} \frac{m_0 + g\overline{\phi}_0}{\sqrt{|\vec{p}|^2 + (m_0 + g\overline{\phi}_0)^2}} f_0(\tau, a|\vec{p}|). \quad (2.19)$$

The evolution equation for φ then reads

$$\frac{\varphi''}{a^2} + 2H \frac{\varphi'}{a} + \left(M^2 + \overline{M}_T^2\right) \varphi + \mathcal{O}(\varphi^2) = \mathcal{O}(H^2 \overline{\phi}_0), \quad (2.20)$$

where \overline{M}_T^2 is given by Eq. (2.17) evaluated for $\phi_0 = \overline{\phi}_0$. That is, the scalar field separates into a component sourced by the fermions, Eq. (2.19); and a fastly oscillating component, satisfying Eq. (2.20). The latter corresponds to a background of ϕ particles at rest, and it is nonzero only if set by the initial condition (up to small corrections $\mathcal{O}\left(\frac{H^2}{M^2 + \overline{M}_T^2}\right)$). Since, on top of that, it does not affect the scalar field sourced by the fermions $\overline{\phi}_0$, we will not study it. In what follows, to simplify notation ϕ_0 will refer to $\overline{\phi}_0$, and M_T^2 to \overline{M}_T^2 .

2.1.2 Solution for a Thermal Fermion Relic

To compute the scalar field ϕ_0 and obtain the macroscopic properties of the system, we have to specify the fermion distribution function f_0 . To this purpose, we will assume that the fermions were in the past in thermal equilibrium. As we are neglecting collisions, they must thermally decouple before long range effects become relevant, i.e., while still relativistic. In this case, we can assume that the fermion distribution function takes a Fermi-Dirac form,

$$f_0(\tau, a|\vec{p}|) = \frac{\mathbf{g}}{(2\pi)^3} \frac{1}{e^{|\vec{p}|/T(a)} + 1}. \quad (2.21)$$

Here, \mathbf{g} is the amount of internal degrees of freedom of the fermion (including particles, antiparticles and any internal quantum number) and T its temperature. The Boltzmann equation (2.15) then requires $T \propto \frac{1}{a}$. This distribution applies, e.g., to neutrinos and other hot thermal relics. Exceptions include particles that never reach thermal equilibrium (e.g., produced through freeze-in) or non-negligible chemical potentials.

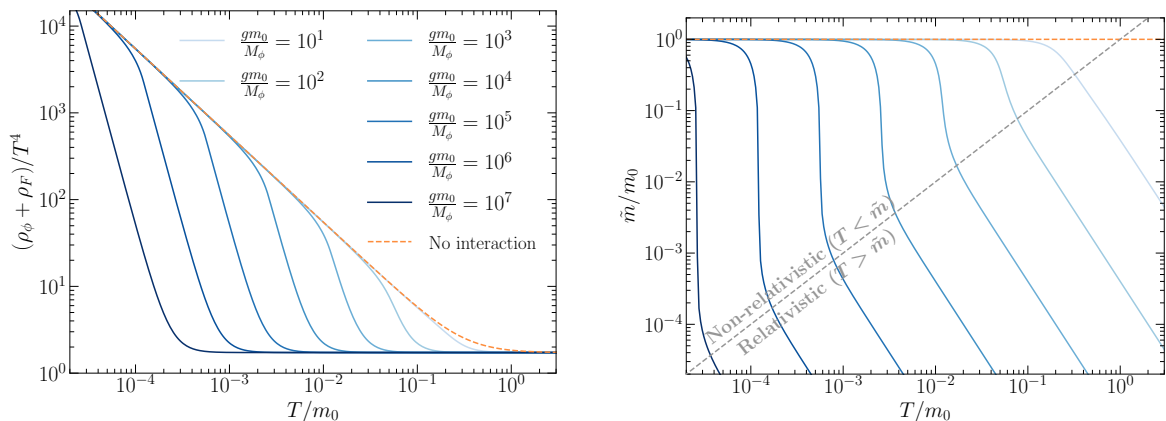
Using Eq. (2.21), we can self-consistently solve Eq. (2.19) to obtain the scalar field ϕ_0 sourced by the fermions. Then, we can compute the effective fermion mass $\tilde{m} = m_0 + g\phi_0$ as well as the energy density ρ and pressure P of the system

$$\rho = \rho_\phi + \rho_F = \frac{1}{2} M_\phi^2 \phi_0^2 + \int d^3\vec{p} \sqrt{|\vec{p}|^2 + \tilde{m}^2} f_0(\tau, a|\vec{p}|), \quad (2.22)$$

$$P = P_\phi + P_F = -\frac{1}{2} M_\phi^2 \phi_0^2 + \int d^3\vec{p} \frac{|\vec{p}|}{3\sqrt{|\vec{p}|^2 + \tilde{m}^2}} f_0(\tau, a|\vec{p}|). \quad (2.23)$$

We have checked that, under our assumption $M_\phi^2 + M_T^2 \gg H^2$, the kinetic term $\frac{1}{2}\dot{\phi}_0^2$ in ρ_ϕ and P_ϕ can be neglected.

From Eq. (2.19), one can see that g and M_ϕ only enter into the homogeneous and isotropic results through the combination $\frac{gm_0}{M_\phi}$. Thus, we show in Fig. 2 for different values of $\frac{gm_0}{M_\phi}$ the energy density ρ (normalized to T^4) as well as the effective fermion mass \tilde{m} (normalized to its vacuum mass m_0) as a function of T (normalized to m_0). We have chosen $\mathbf{g} = 6$, so that our results directly apply to three interacting neutrino and antineutrino species.



(a) Energy density of the system divided by T^4 .

(b) Effective fermion mass divided by m_0 . The gray line separates the non-relativistic and relativistic regimes.

Figure 2: Energy density and effective fermion mass as a function of T/m_0 for different interaction strengths [solid blue shades]. The dashed orange line shows the result without long range interactions. T is the fermion temperature, m_0 its vacuum mass, and $\frac{gm_0}{M_\phi}$ parametrizes the interaction strength. The fermion distribution function is given by Eq. (2.21) with $\mathbf{g} = 6$ degrees of freedom.

Figure 2 allows to understand the cosmological evolution of the system. In the very early Universe ($T \gg m_0$) all fermions are ultrarelativistic and, as seen in the rightmost side of Fig. 2a, the energy density of the system is that of a non-interacting gas of ultrarelativistic fermions. As the Universe expands, the temperature decreases and for strong enough interactions the sourced scalar field reduces the effective fermion mass (see Fig. 2b), keeping fermions relativistic even though $T \ll m_0$. Therefore, they will contribute to the energy density as $\rho_F \propto T^4$. As we will see, the scalar field contribution is independent of T , so at some point it takes over the fermion contribution, giving the steeply increasing energy density seen in Fig. 2a. Finally, when the temperature is small enough, the interparticle distance is larger than the interaction range and all interaction effects switch off: the energy density is that of a non-interacting gas of fermions, and $\tilde{m} = m_0$.

The rate at which the energy density changes can be quantified through the equation of state parameter $w \equiv P/\rho$, as in an expanding Universe $\frac{1}{\rho} \frac{d\rho}{dt} = -3H(1+w)$. This is shown in Fig. 3 as a function of the fermion temperature T (normalized to its vacuum mass m_0) for different interaction strengths. As we can see, for $T \gg m_0$ there are no interaction effects and the equation of state is that of an ideal gas of non-interacting relativistic fermions, $w = 1/3$. As the temperature decreases, the interaction keeps fermions ultrarelativistic, and w is still $1/3$ until the scalar field energy density and pressure take over those of the fermions. At this point, the equation of state parameter can take negative values, even reaching $w \simeq -1$.

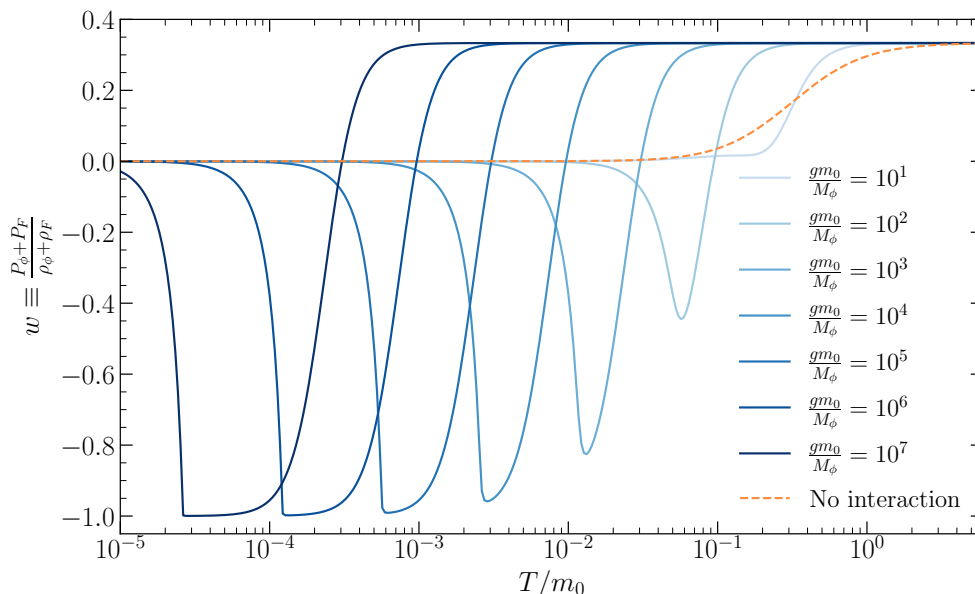


Figure 3: Equation of state of the system as a function of T/m_0 for different interaction strengths [solid blue shades]. The dashed orange line shows the result without long range interactions. T is the temperature, m_0 the vacuum fermion mass, and $\frac{gm_0}{M_\phi}$ parametrizes the interaction strength. The fermion distribution function is given by Eq. (2.21) with $\mathfrak{g} = 6$ degrees of freedom.

Finally, as the system cools down the interparticle distance gets larger than the interaction range and all interaction effects switch off. The equation of state is then that of a non-interacting gas of non-relativistic fermions, $w = 0$.

The behavior in Figs. 2 and 3 can be analytically understood by approximately solving Eq. (2.19). If $T \gg \tilde{m}$, we can neglect the second term in the square root and

$$\phi_0 \simeq -\frac{\frac{\mathfrak{g}}{24}g\frac{m_0}{T}T^3}{M_\phi^2 + \frac{\mathfrak{g}}{24}g^2T^2} = -\frac{g}{M_\phi^2} \frac{\tilde{m}}{T} \frac{\mathfrak{g}}{24}T^3, \quad (2.24)$$

$$\tilde{m} \simeq m_0 \frac{1}{1 + \frac{\mathfrak{g}}{24} \frac{g^2T^2}{M_\phi^2}}. \quad (2.25)$$

In this limit, the scalar field ϕ_0 is simply proportional to the product of the coupling g ; a factor $\frac{m_0}{T}$ that, as we anticipated, suppresses long range effects for $T \gg m_0$; and T^3 , proportional to the fermion number density. In the denominator, we have the effective scalar mass squared $M_{\text{eff}}^2 \equiv M_\phi^2 + M_T^2 \simeq M_\phi^2 + \frac{\mathfrak{g}}{24}g^2T^2$, that enhances ϕ_0 for longer interaction ranges (i.e., smaller scalar masses). Notice that the naive enhancement of the interaction by reducing M_ϕ to increase its range is only effective until $M_\phi \lesssim M_T$. Finally, from Eq. (2.25) we see that as long as $\frac{\mathfrak{g}}{24} \frac{g^2T^2}{M_\phi^2} \gg \frac{m_0}{T}$, the sourced scalar field keeps the fermions ultrarelativistic.

We can also analytically understand why in Fig. 3 there is a region with a dark energy-like equation of state, $w \simeq -1$. Using Eq. (2.25), we can write $\phi_0 \propto \frac{\tilde{m}}{T}T^3$. For high enough temperatures, $\frac{\tilde{m}}{T} \sim \frac{1}{T^3}$, and so the scalar field stays constant as the Universe expands. In other words, the decrease of long range effects due to the dilution of the fermions is exactly compensated by them becoming less relativistic.

On the other hand, for $T \ll \tilde{m}$ (which, as we have seen above, requires $\frac{\mathfrak{g}}{24} \frac{g^2 T^2}{M_\phi^2} \lesssim \frac{m_0}{T}$),

$$\phi_0 \simeq -\frac{3\zeta(3)\mathfrak{g}}{4\pi^2} g \frac{T^3}{M_\phi^2}, \quad (2.26)$$

$$\tilde{m} \simeq m_0 \left(1 - \frac{3\zeta(3)\mathfrak{g}}{4\pi^2} \frac{g^2 T^2}{M^2} \frac{T}{m_0} \right). \quad (2.27)$$

That is, ϕ_0 is the product of the coupling and the fermion number density divided by the vacuum scalar mass squared (as in this limit M_T is negligible). As the temperature decreases, the scalar field energy density dilutes as T^6 , whereas the fermion energy density dilutes slower, as T^3 . At the same time, fermions rapidly acquire their vacuum mass. In other words, all the long range effects rapidly turn off as intuitively expected from an interaction whose energy density is proportional to the fermion number density squared.

2.2 Perturbations and Instability

After having discussed the evolution of a homogeneous and isotropic background, the next step to characterize the cosmology of a system of long range interacting fermions is to study linear inhomogeneous perturbations. In the following, we will work in the synchronous gauge [84]

$$ds^2 = a(\tau)^2 [-d\tau^2 + (\delta_{ij} + h_{ij}(\vec{x}, \tau)) dx^i dx^j]. \quad (2.28)$$

We will only consider scalar metric perturbations, that can be Fourier expanded as

$$h_{ij}(\vec{x}, \tau) = \int d^3k e^{i\vec{k}\cdot\vec{x}} \left[\hat{k}_i \hat{k}_j h(\vec{k}, \tau) + \left(\hat{k}_i \hat{k}_j - \frac{1}{3} \delta_{ij} \right) 6\eta(\vec{k}, \tau) \right], \quad (2.29)$$

where $\hat{k} \equiv \frac{\vec{k}}{|\vec{k}|}$ and $h(\vec{k}, \tau)$ and $\eta(\vec{k}, \tau)$ are the scalar metric perturbations in Fourier space. In addition, we will write the fermion distribution function and scalar field as

$$f(x^\mu, P_\mu) = f_0(\tau, q) [1 + \Psi(\vec{x}, \tau, q, \hat{n})], \quad (2.30)$$

$$\phi(x^\mu) = \phi_0(\tau) + \delta\phi(\vec{x}, \tau), \quad (2.31)$$

where $\hat{n} \equiv \frac{\vec{p}}{|\vec{p}|}$.

The Boltzmann equation (2.8) in Fourier space reads, to linear order in perturbations,

$$\Psi' + i \frac{q}{\varepsilon} (\vec{k} \cdot \hat{n}) \Psi + \frac{d \log f_0}{d \log q} \left[\eta' - \frac{h' + 6\eta'}{2} (\hat{k} \cdot \hat{n})^2 - g \frac{a^2 \tilde{m}}{q\varepsilon} i(\vec{k} \cdot \hat{n}) \delta\phi \right] = 0, \quad (2.32)$$

where $\varepsilon \equiv \sqrt{q^2 + \tilde{m}^2 a^2}$. The term in square brackets corresponds to the effect of long range interactions, either gravitational, parametrized by η and h ; or induced by the scalar field, proportional to $g \vec{p} \cdot \vec{\nabla} \delta\phi \sim g(\hat{k} \cdot \hat{n}) \delta\phi$ and suppressed by $\frac{\tilde{m}}{\varepsilon}$ for ultrarelativistic fermions. Finally, we can expand Ψ in Legendre polynomials following the conventions in Ref. [84], obtaining the following tower of Boltzmann equations

$$\Psi'_0 = -\frac{qk}{\varepsilon} \Psi_1 + \frac{1}{6} h' \frac{d \log f_0}{d \log q}, \quad (2.33)$$

$$\Psi'_1 = \frac{qk}{3\varepsilon} (\Psi_0 - 2\Psi_2) - g \frac{a^2 \tilde{m} k}{3q\varepsilon} \delta\phi \frac{d \log f_0}{d \log q}, \quad (2.34)$$

$$\Psi'_2 = \frac{qk}{5\varepsilon} (2\Psi_1 - 3\Psi_3) - \left(\frac{1}{15} h' + \frac{2}{5} \eta' \right) \frac{d \log f_0}{d \log q}, \quad (2.35)$$

$$\Psi'_\ell = \frac{qk}{(2\ell + 1)\varepsilon} [\ell \Psi_{\ell-1} - (\ell + 1) \Psi_{\ell+1}] \quad \forall \ell \geq 3. \quad (2.36)$$

That is, the effect of long range interactions enters both through a time-dependent mass \tilde{m} as well as through an interaction with scalar field perturbations in the $\ell = 1$ multipole.

Regarding the equation for the scalar field (2.7), it reads in Fourier space to linear order

$$\delta\phi'' + 2aH\delta\phi' + \frac{1}{2}h'\phi' + [k^2 + a^2(M_\phi^2 + M_T^2)]\delta\phi = -g4\pi \int dq q^2 \frac{\tilde{m}}{\varepsilon} f_0(q)\Psi_0(q, k, \tau). \quad (2.37)$$

As in Section 2.1.1, if the effective inverse scalar mass $[(k/a)^2 + M_\phi^2 + M_T^2]^{-1/2}$ is much smaller than other timescales, we can apply the adiabatic approximation and

$$[(k/a)^2 + M_\phi^2 + M_T^2]\delta\phi \simeq -g\frac{4\pi}{a^2} \int dq q^2 \frac{\tilde{m}}{\varepsilon} f_0(q)\Psi_0(q, k, \tau). \quad (2.38)$$

From Eqs. (2.32) and (2.38), we see that the scalar interaction will introduce a new attractive long range force among fermions. If it is stronger than or comparable to gravity, it can significantly affect structure growth, as first pointed out in Ref. [99] in the context of neutrino-induced dark energy models (see also Refs. [100–103]).

In particular, Ref. [99] found that for scalar masses $M_{\text{eff}} \gg H$, as in our case, non-relativistic fermion density perturbations of sizes $\gtrsim M_{\text{eff}}^{-1}$ exponentially grow over timescales $\ll M_{\text{eff}}^{-1}$ much shorter than cosmological times. As a consequence, when becoming non-relativistic, all fermions will collapse into non-linear structures or *nuggets* with typical sizes $< M_{\text{eff}}^{-1}$, separated by distances $\gg M_{\text{eff}}^{-1}$. The outcome of this transition will be a dilute gas of non-interacting *nuggets*, with sizes much smaller than cosmological scales, behaving as dust.

Following Ref. [102], we have computed the interaction strengths in our model for which fermion density perturbations exponentially grow (see Appendix B for the details). Our results are depicted in Fig. 4, where we show in shaded the values of $\frac{gm_0}{M_\phi}$ and temperature (in units of the effective fermion mass \tilde{m}) where this instability is present. As we see, for interactions strengths $\frac{gm_0}{M_\phi} \gtrsim 5$, as soon as fermions become non-relativistic ($T \lesssim 0.8\tilde{m}$) the long range interaction makes perturbations quickly grow. For $T > \tilde{m}$, perturbations do not grow due to two effects: on the one hand, the large dispersion velocities of relativistic particles inhibit perturbation growth; on the other hand, scalar interactions are suppressed for relativistic fermions. Notice that the second effect is characteristic of our model and is not generically present for other interactions. In addition, for small $\frac{gm_0}{M_\phi}$, when fermions become non-relativistic the interparticle distance is larger than the interaction range and the scalar self interaction does not induce perturbation growth.

In order to model this instability, we quantify in Appendix B the timescale over which fermion density perturbations become non-linear due to the exponential growth. This timescale is much smaller than cosmological scales as long as

$$\sqrt{M_\phi^2 + M_T^2} \gtrsim 10^5 H. \quad (2.39)$$

We will impose this condition, and consider that as soon as the temperature drops below the unstable temperature in Fig. 4,⁵ the system undergoes an instantaneous transition to a dust-like behavior. Under this assumption, the energy density and equation of state of the fermion background as a function of temperature⁶ are shown in Fig. 5. As we see, the transition takes

⁵We have checked that the final results are not sensitive to the specific temperature at which the system becomes unstable within $\lesssim 10\%$ variations of the latter.

⁶Technically, the fermion temperature is not well defined after *nugget* formations, as the fermion background does not have a thermal distribution. In this region, T should be understood as a proxy for the scale factor.

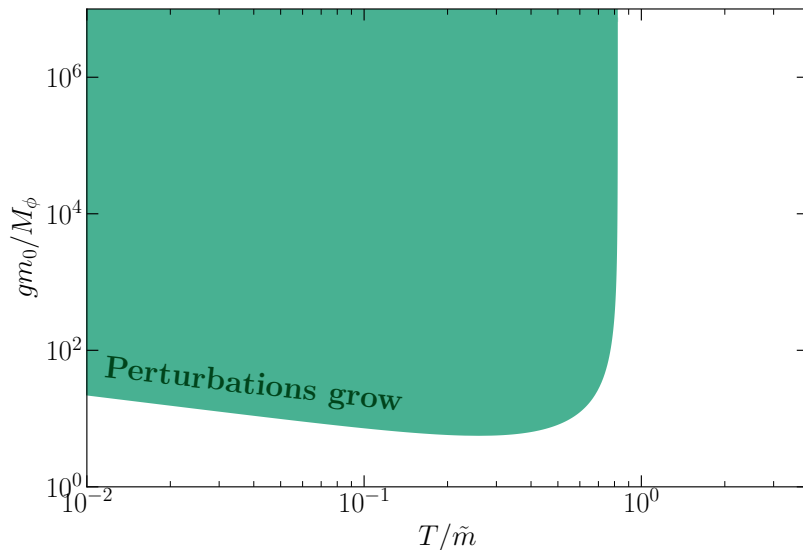


Figure 4: The green region shows the values of the interaction strength $\frac{gm_0}{M_\phi}$ and temperature T (in units of the effective fermion mass \tilde{m}) where perturbations grow due to the long range interaction. For large temperatures, relativistic motion inhibits perturbation growth. Below the green region, perturbations do not grow because the relevant interaction range is shorter than the average interparticle distance. The fermion distribution function is given by Eq. (2.21) with $\mathfrak{g} = 6$ degrees of freedom.

place relatively late and most of the phenomenology described in Section 2.1 is still valid. Furthermore, the low temperature energy density now depends on the interaction strength, as the latter controls the instant of *nugget* formation.

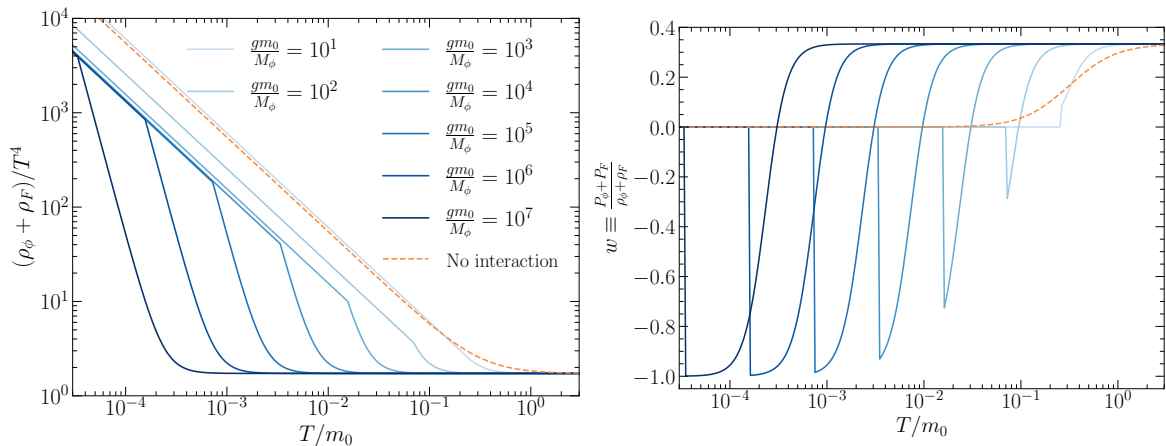


Figure 5: Energy density [left] and equation of state [right] of the system for different interactions strengths [solid blue shades], including instantaneous *nugget* formation. See Figs. 2 and 3 and text for details. The fermion distribution function is given by Eq. (2.21) with $\mathfrak{g} = 6$ degrees of freedom.

If Eq. (2.39) does not hold, the timescale of fermion density perturbation growth can

be comparable to cosmological scales. As M_{eff} gets smaller, the long range interaction will generically compete with gravity, leading to effects on LSS. In addition, as discussed in Section 2.1.1, the background will behave like quintessence and depend on the initial value of the scalar field. Both scenarios have been widely studied in the literature [6–13, 91–98].

3 Cosmological Observables and Data Analysis: Neutrinos as a Benchmark

As discussed in the Introduction, we will now explore the observational consequences for neutrinos of the physics developed in Section 2. From the results in that Section, we conclude that neutrinos are particularly well suited to study the cosmology of long range interactions. On the one hand, scalar long range interaction effects start being relevant when the fermion temperature drops below its mass. For neutrinos, this generically happens relatively late in the cosmological history, at times from which we have precise observations. On the other hand, cosmology claims to be sensitive to the absolute neutrino mass scale, although cosmological observations do not kinematically measure the neutrino mass. As neutrinos decouple from the primordial plasma relatively early, CMB and LSS observations are only sensitive to their gravitational impact. That is, their energy density and how it changes as the Universe expands (i.e., their equation of state). This depends on the neutrino mass in an assumption-dependent way [70, 71], and we expect this measurement to be affected by the modified equation of state induced by long range interactions (see Fig. 5).

For simplicity, we will consider a single scalar field universally coupled to all three neutrino mass eigenstates, which we assume to be degenerate in mass with individual masses m_0 . As discussed in Section 2.1.1, we are interested in studying the regime where neutrino-neutrino scatterings can be neglected, and when the scalar mass M_{eff} is much larger than the Hubble parameter. The former assumption corresponds to coupling constants $g \lesssim 10^{-7}$ [34], guaranteeing that the neutrino momentum distribution is the same as in the Standard Model. To a good approximation, this corresponds to a Fermi-Dirac distribution with negligible chemical potentials and a present day temperature $T_\nu \simeq 0.716 T_\gamma$ [104–108] with T_γ the photon temperature. For $g \lesssim 10^{-7}$, $\frac{gm_0}{M_\phi} > 1$ and $m_0 \sim 0.1 \text{ eV}$; $M_{\text{eff}} \gg H$ at the relevant temperatures $T \lesssim m_0$ implies $10^{-8} \text{ eV} \gtrsim M_\phi \gtrsim 10^{-25} \text{ eV}$. These ~ 17 orders of magnitude in mediator mass have not been systematically studied in the literature and, as we will see, they can impact cosmological observations.

Regarding laboratory constraints, couplings $g \lesssim 10^{-7}$ are well allowed [23–29, 109]. Nevertheless, for small M_ϕ long range interactions may affect neutrino oscillation data. On the one hand, the cosmic neutrino background could reduce the present day effective neutrino mass below the minimum value allowed by oscillations. On the other hand, the large neutrino number density in the Sun could reduce the effective neutrino mass, modifying solar neutrino data [110–112].⁷ Both effects are relevant only for $\frac{g}{M_\phi} \gtrsim 10^5\text{--}10^6 \text{ eV}^{-1}$ and, furthermore, they can be easily avoided by modifying the flavor structure of the scalar-neutrino coupling. Therefore, we will mostly ignore them in what follows.

In this Section, we will study the impact of neutrino long range interactions on CMB anisotropies, Baryon Acoustic Oscillation (BAO) data, and future LSS observations. We will start by qualitatively understanding the physical effects. We will then perform a Bayesian

⁷This effect can be more important in supernovae due to larger neutrino densities. Current SN1987A data is compatible with massless neutrinos, and thus insensitive to these long range effects, but future observations might be sensitive to them.

analysis of the Planck 2018 TT, TE, EE, lowE, and lensing CMB data [78]; as well as the BAO data from the 6dF galaxy survey [113], the Main Galaxy Sample from the SDSS DR7 [114], and the BOSS-DR12 analysis [115]. Finally, we will study the prospects of adding data from the future Large Scale Structure (LSS) EUCLID survey [60, 63, 116]. To carry out these analyses, we have modified the publicly available CLASS code [117–120] to solve the cosmological perturbation equations with long range interactions (our modification is available [at this URL](#) ) and we have explored the parameter space with the public Markov Chain Monte Carlo (MCMC) code `Monte Python` [121, 122]. All MCMC chains have been run until every Gelman-Rubin coefficient [123] was $R - 1 < 0.02$. Our priors on the model parameters are summarized in Table 1. In particular, the range of $\sum m_\nu$ covers all values allowed by oscillations [124–126] and the latest results from the KATRIN experiment [64]. As we shall see, there are unbounded directions in the $\{\sum m_\nu, g/M_\phi\}$ parameter space. To efficiently explore it, we have chosen logarithmic priors in these parameters, as well as parameter ranges that avoid excessive Bayesian volume effects.

Parameter	Prior	Range	Meaning
ω_b	Linear	$[0, \infty)$	Reduced baryon density parameter
ω_{cdm}	Linear	$[0, \infty)$	Reduced cold dark matter density parameter
θ_s	Linear	$[0, \infty)$	Acoustic CMB angular scale
A_s	Logarithmic	$[0, \infty)$	Primordial power spectrum amplitude at comoving scale $k_0 = 0.05 \text{ Mpc}^{-1}$
n_s	Linear	$[0, \infty)$	Scalar spectral index
τ_{reio}	Linear	$[0.004, \infty)$	Optical depth to reionization
$\sum m_\nu/\text{eV}$	Logarithmic	$[0.024, 3]$	Sum of neutrino masses
$\frac{g}{M_\phi} \times \text{eV}$	Logarithmic	$[10^{-2}, 10^{7.5}]$	Long range interaction coupling divided by the mediator mass

Table 1: Model parameters in our analysis along with their priors, ranges and physical meanings. For a parameter x , “Linear” prior means that we take a uniform prior on x , whereas for “Logarithmic” we take a uniform prior on $\log x$.

3.1 Analysis of Present Data

We begin by qualitatively understanding the main effects of neutrino long range interactions on CMB anisotropies. To this purpose, we show in Fig. 6 the CMB temperature power spectrum for ΛCDM with massless neutrinos (top), as well as its relative difference with respect to a model with long range interacting massive neutrinos with different interaction strengths (bottom). In order to mimic the observable effects, in the bottom panel we have kept fixed the well-measured parameters ω_b , ω_{cdm} , θ_s , A_s , n_s , and τ_{reio} (see Table 1 for the meaning of each parameter). We also show in grey Planck 2018 data [78]. We start by reviewing the main effects of neutrino masses [127] (dashed orange line in Fig. 6):

- *The Integrated Sachs-Wolfe (ISW) effect.* This arises because, after leaving the last scattering surface, CMB photons traverse gravitational potential wells. Because of gravitational growth and the expansion of the Universe, the depth of the wells may change while photons are inside them. Therefore, the net gravitational redshift of photons after entering and exiting the wells may be non zero.

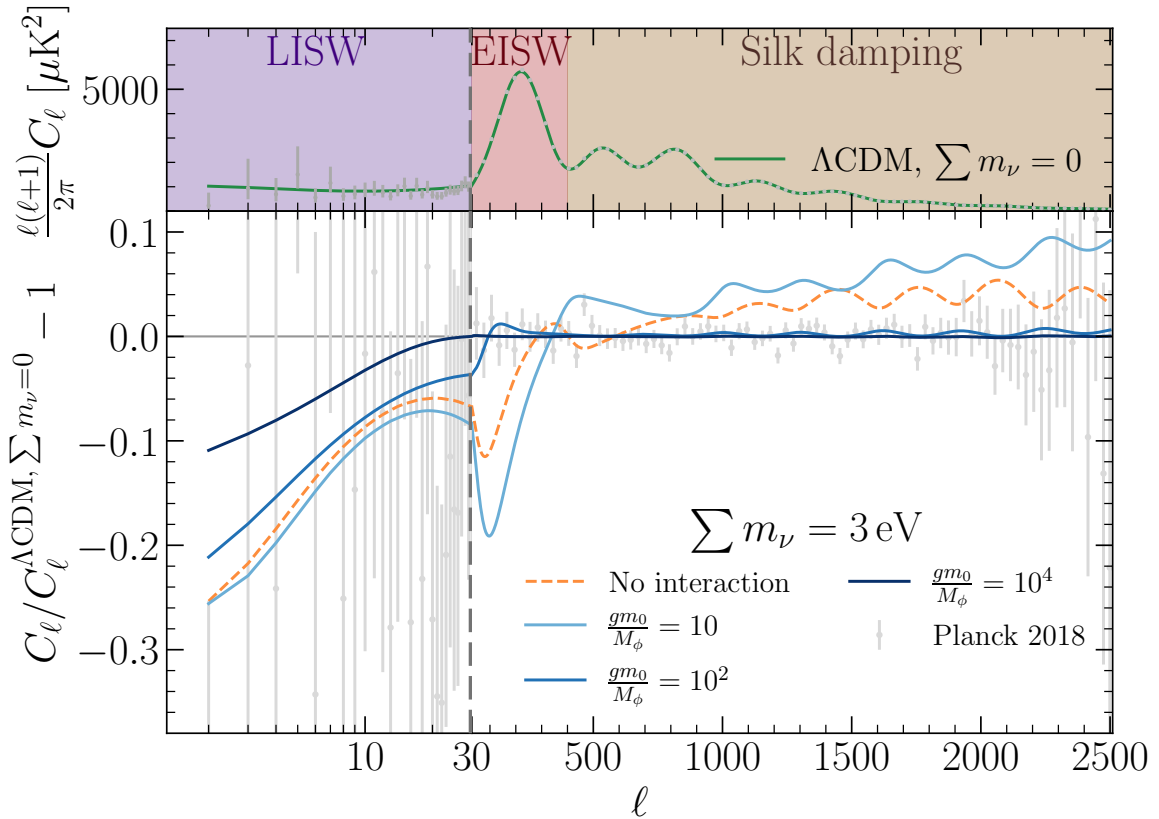


Figure 6: Top: CMB temperature power spectrum for Λ CDM with massless neutrinos [solid] and Planck 2018 data [78]. We show in shaded the multipole ℓ ranges where the Late Integrated Sachs-Wolfe effect (LISW), Early Integrated Sachs-Wolfe effect (EISW), and Silk damping leave their main imprints. Bottom: relative difference of the power spectrum between Λ CDM with massless neutrinos, and massive neutrinos with long range interactions. For the latter, we have chosen $\sum m_\nu = 3$ eV and different interaction strengths [solid blue shades]. We also show the result without interactions [dashed orange] as well as Planck 2018 data [grey].

This effect depends on the expansion rate of the Universe, i.e., on its equation of state. It exactly vanishes for a fully matter dominated Universe, and is generically non-zero at two times: just after recombination, when the Universe still contains a non-negligible amount of radiation (Early Integrated Sachs-Wolfe, or EISW, effect); and at late times when the cosmological constant Λ starts being relevant (Late Integrated Sachs-Wolfe, or LISW, effect).

The contribution of neutrino masses to the LISW effect can be understood as follows. When neutrinos become non-relativistic, their energy density redshifts slower as their equation of state changes from radiation ($w = 1/3$) to dust ($w = 0$). Therefore, they will contribute more to the expansion of the Universe. This would modify the well-measured angular scale of the CMB peaks, $\theta_s = \left[\int_{z_{\text{rec}}}^{\infty} c_s(z) \frac{dz}{H(z)} \right] \times \left[\int_0^{z_{\text{rec}}} \frac{dz}{H(z)} \right]^{-1}$ with z_{rec} the recombination redshift and c_s the speed of sound of the primordial plasma, and

can be compensated for by changing Λ and therefore modifying the LISW effect. This is visible in the low ℓ region of Fig. 6.

Similarly, the EISW effect measures how the equation of state of the Universe deviates from $w = 0$ close to recombination. If neutrinos become non-relativistic early enough, their contribution to the EISW effect will be reduced: this is visible for $\ell \sim 200$ in Fig. 6.

- *Silk damping.* Due to the non-zero photon mean free path, perturbations at small angular scales (large ℓ) are exponentially damped. The characteristic angular scale of this damping, $\theta_D \propto \sqrt{\int_{z_{\text{rec}}}^{\infty} \frac{1}{a(z)n_e(z)H(z)} dz}$ with n_e the free electron number density, depends on the neutrino contribution to the expansion of the Universe before recombination. Thus, if neutrinos become non-relativistic before recombination, their energy density redshifts slower, they contribute more to $H(z)$, and the damping scale gets reduced. This is visible at large ℓ in Fig. 6.

We therefore conclude that the CMB measurement of neutrino masses is mostly a measurement of their equation of state as a function of redshift. Thus, the non-trivial equation of state that our model introduces (see Fig. 5) will affect the same three CMB features discussed above. This is visible in Fig. 6: for $\frac{gm_0}{M_\phi} = 10$ neutrinos behave as dust earlier, enhancing the effects of neutrino masses; for $\frac{gm_0}{M_\phi} = 10^2$ there is a period where $w < 0$ and therefore the EISW effect is enhanced, contrarily to the effect of massive neutrinos; and for $\frac{gm_0}{M_\phi} = 10^4$ the neutrino system behaves as radiation before recombination, removing the EISW and Silk damping effects of neutrino masses. We anticipate from these results that large interaction strengths will significantly affect the cosmological bound on neutrino masses, as they delay and modify the $w = 1/3$ to $w = 0$ transition. A similar effect was explored in Refs. [70, 71], where this transition changed due to a non-thermal neutrino distribution function.

Moving on to the data analysis, we show in Fig. 7 the results of analyzing Planck CMB observations. In solid, we show the 1-D posterior probabilities and the marginalized 2-D 2σ credible regions for the parameters that are most affected by our modification to Λ CDM: the sum of neutrino masses $\sum m_\nu$, the interaction strength as parametrized by $\frac{g}{M_\phi}$, the Hubble constant H_0 , and the amplitude parameter σ_8 . In dotted, we show the results assuming Λ CDM with massive neutrinos; and in the hatched region cosmic neutrinos would still be relativistic today. As discussed before, a priori the hatched region is in conflict with neutrino oscillation measurements, although simple modifications of the coupling structure could accommodate this data. The dark green line is the minimum value of $\sum m_\nu$ allowed by neutrino oscillation data [124–126]. For completeness, we show in Appendix C the posterior probabilities and credible regions for all parameters in our analysis.

As we see, no neutrino mass bound can be obtained from CMB data if the interaction is strong enough to delay the relativistic to non-relativistic equation of state transition (see Fig. 2b): for $g/M_\phi \gtrsim 10^2 \text{ eV}^{-1}$, the neutrino system still behaves as radiation at recombination. For small couplings $g/M_\phi \lesssim 10 \text{ eV}^{-1}$, we essentially recover the standard cosmology and neutrino mass bound. Because of this, for $\sum m_\nu \gtrsim 0.1 \text{ eV}$ interaction strengths $g/M_\phi \lesssim 10 \text{ eV}^{-1}$ are excluded.

We also observe that H_0 and σ_8 are quite correlated with the neutrino mass and interaction strength. The correlation with $\sum m_\nu$ is also present in the standard Λ CDM scenario [dotted orange], and is due to the late time contribution of massive neutrinos to the energy

density of the Universe. The correlation with g/M_ϕ , in turn, gets reduced at large couplings. This is because for such couplings our attractive self interaction reduces the energy density in neutrinos, partly due to *nugget* formation (see Fig. 5).

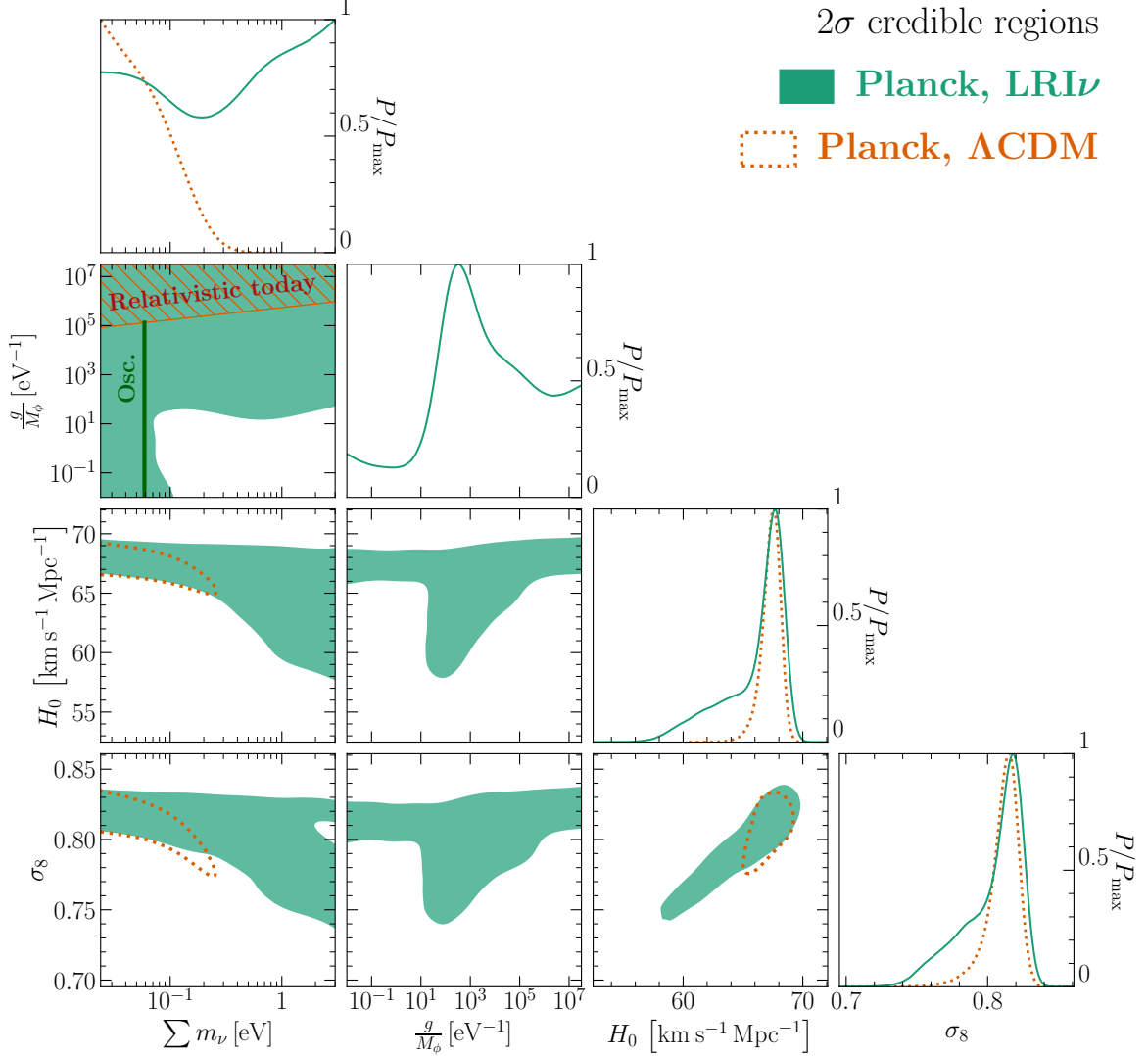


Figure 7: Planck 2018 constraints [78] on long range interacting neutrinos, LRI ν , [solid light green] and on Λ CDM with non-interacting massive neutrinos [dotted orange]. We show the marginalized 2σ credible regions and 1-D posterior probability distributions for the most relevant parameters. For $\sum m_\nu$ and $\frac{g}{M_\phi}$, posteriors are constructed with uniform logarithmic bins. In the hatched region, cosmic neutrinos are relativistic today. The dark green line is the minimum value of $\sum m_\nu$ allowed by neutrino oscillation data [124–126].

The allowed parameter values in Fig. 7 have essentially the same cosmological history before recombination: neutrinos behaving as radiation. As they differ in their post-recombination behavior, we expect late time cosmological probes to be sensitive to a region of parameter space allowed by Planck data.

LSS measurements are a standard but powerful example of such probes. They contain

many rich features, sensitive both to the late-time structure growth and to the expansion history of the Universe. Furthermore, there are very precise present observations available that will significantly improve in the near future [60, 113–115, 128–133]. As the goal of this work is not to carry out a detailed study of the complementarity among different datasets, we will only use BAO results for our analysis of present data. These are accurate and generically accepted to be robust against systematic uncertainties and changes in the underlying cosmological model. Including other LSS probes may require a more careful treatment of the data and the systematic uncertainties. Furthermore, our scenario and non-interacting massive neutrinos induce similar features in the matter power spectrum. Including additional LSS data does not significantly improve the neutrino mass bound [78], partially due to small tensions with Planck, and so we don't expect it to change our conclusions regarding neutrino long range interactions.

BAO measurements are mostly sensitive to

$$\frac{D_V}{r_s^{\text{drag}}}(z) = \frac{\left[\frac{z}{H(z)} \left(\int_0^z \frac{dz'}{H(z')} \right)^2 \right]^{1/3}}{\int_{z_{\text{drag}}}^{\infty} c_s(z') \frac{dz'}{H(z')}} , \quad (3.1)$$

with z_{drag} the baryon drag redshift. We show in Fig. 8 this quantity as a function of redshift for two scenarios: Λ CDM with massless neutrinos, and Λ CDM with massive self-interacting neutrinos. For the latter, we have chosen $\sum m_\nu = 1 \text{ eV}$ and $\frac{g}{M_\phi} = 10^2 \text{ eV}^{-1}$, parameter values allowed by Planck data (see Fig. 7) for which neutrinos behave as radiation before recombination. The difference between both curves is therefore due to the neutrino contribution to the late time energy density of the Universe, and thus to the late time Hubble parameter in Eq. (3.1). We also show observational data from Refs. [113–115], in clear tension with the self-interacting neutrino scenario.

Regarding the full data analysis, we show in Fig. 9 the 1-D posterior probabilities and the marginalized 2-D 2σ credible regions including Planck 2018 and BAO observations [78, 113–115] for $\sum m_\nu$, $\frac{g}{M_\phi}$, H_0 , and σ_8 . We show in solid the results assuming Λ CDM with massive self-interacting neutrinos, in dotted for Λ CDM with massive neutrinos without self interactions, in dashed for Λ CDM with massive self-interacting neutrinos but without BAO data (i.e., the light green lines in Fig. 7), and in the hatched region cosmic neutrinos would still be relativistic today. The dark green line is the minimum value of $\sum m_\nu$ allowed by neutrino oscillation data [124–126]. For completeness, we show in Appendix C the posterior probabilities and credible regions for all parameters in our analysis.

As we see, BAO data excludes a large amount of interaction strengths for relatively large values of the neutrino mass. As discussed above, this is due to the dependence of the late time neutrino energy density on $\sum m_\nu$ and g/M_ϕ , partly due to *nugget* formation (see Fig. 5). Excluding a large amount of interaction strengths also breaks the degeneracies with H_0 and σ_8 , giving essentially the same results as Λ CDM for these parameters. Nevertheless, there is still no cosmological neutrino mass bound.

In other words, the KATRIN laboratory experiment, that aims to constraint $\sum m_\nu \lesssim 0.6 \text{ eV}$ [64], could in the near future detect a non-zero neutrino mass compatible with cosmology for interaction strengths $g/M_\phi \sim 10^3\text{--}10^6 \text{ eV}^{-1}$.

Notice that, especially after introducing BAO data, long range interacting neutrinos do

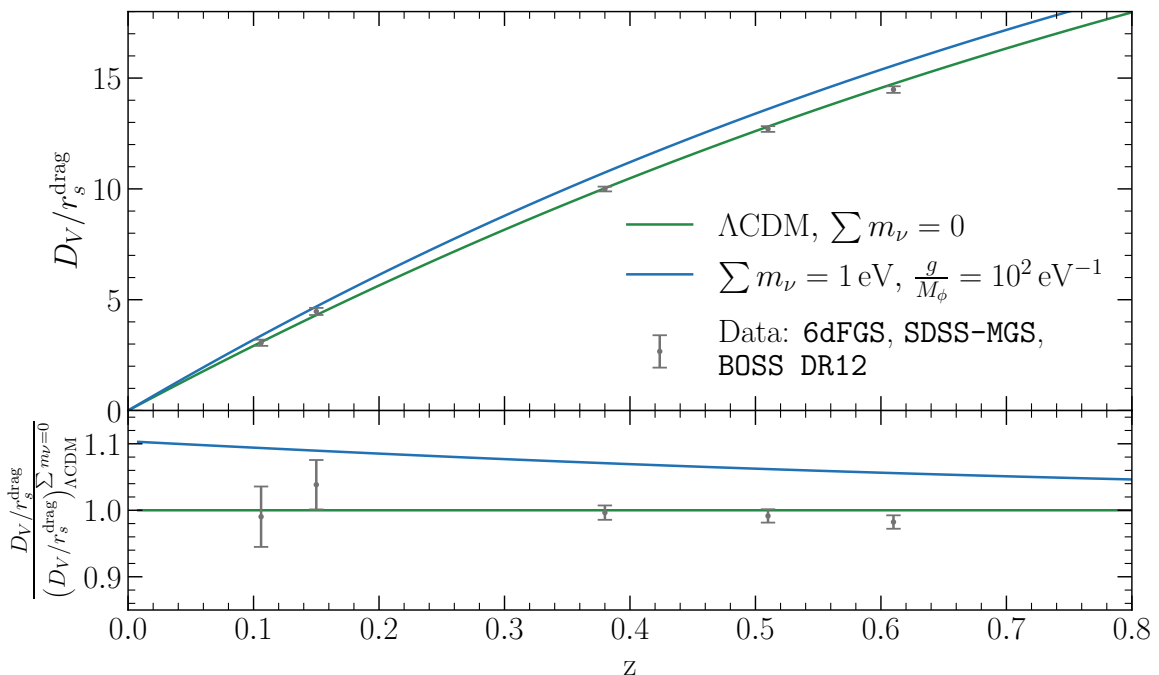


Figure 8: Top: BAO scale for Λ CDM with massless neutrinos [green], with a model of self-interacting massive neutrinos allowed by Planck data [blue], and observational data [113–115]. Bottom: ratios with respect to Λ CDM with massless neutrinos. To generate the solid curves, we have fixed ω_b , ω_{cdm} , θ_s , A_s , n_s , and τ_{reio} .

not solve the H_0 tension (see Ref. [134] for an overview of the tension and proposed solutions).⁸ This can be understood from Fig. 5: this tension is generically solved by increasing the energy density of the Universe around recombination, but a scalar interaction, being universally attractive, will *reduce* the energy.

3.2 Future Prospects for Large Scale Structure

As we have just discussed, since neutrinos become non-relativistic relatively late, late time cosmological measurements are generically quite sensitive to neutrino long range interactions. In the previous subsection, we have illustrated this point with BAO data, a precise feature of the matter power spectrum that is considered to be robust. The situation should further improve in the near future, when surveys such as EUCLID [60] aim to precisely measure the full power spectrum at different redshifts. In the following, we will study the impact of long range interacting neutrinos on the matter power spectrum, as well as the implications of future EUCLID data.

We start by illustrating in Fig. 10 the relative difference in matter power spectrum between Λ CDM with massless neutrinos, and Λ CDM with self-interacting massive neutrinos for different masses and long range interaction strengths. In dashed orange, neutrinos do not self interact and have the smallest mass allowed by oscillation data. The solid blue lines correspond to different parameters allowed by Planck and BAO data (see Fig. 9).

⁸As can be seen from Fig. 14, the posteriors for Ω_m and σ_8 are essentially the same as in Λ CDM. Thus, we expect the parameter $S_8 \equiv \sigma_8 \sqrt{\Omega_m/0.3}$ and its associated tension [78] not to be affected by neutrino long

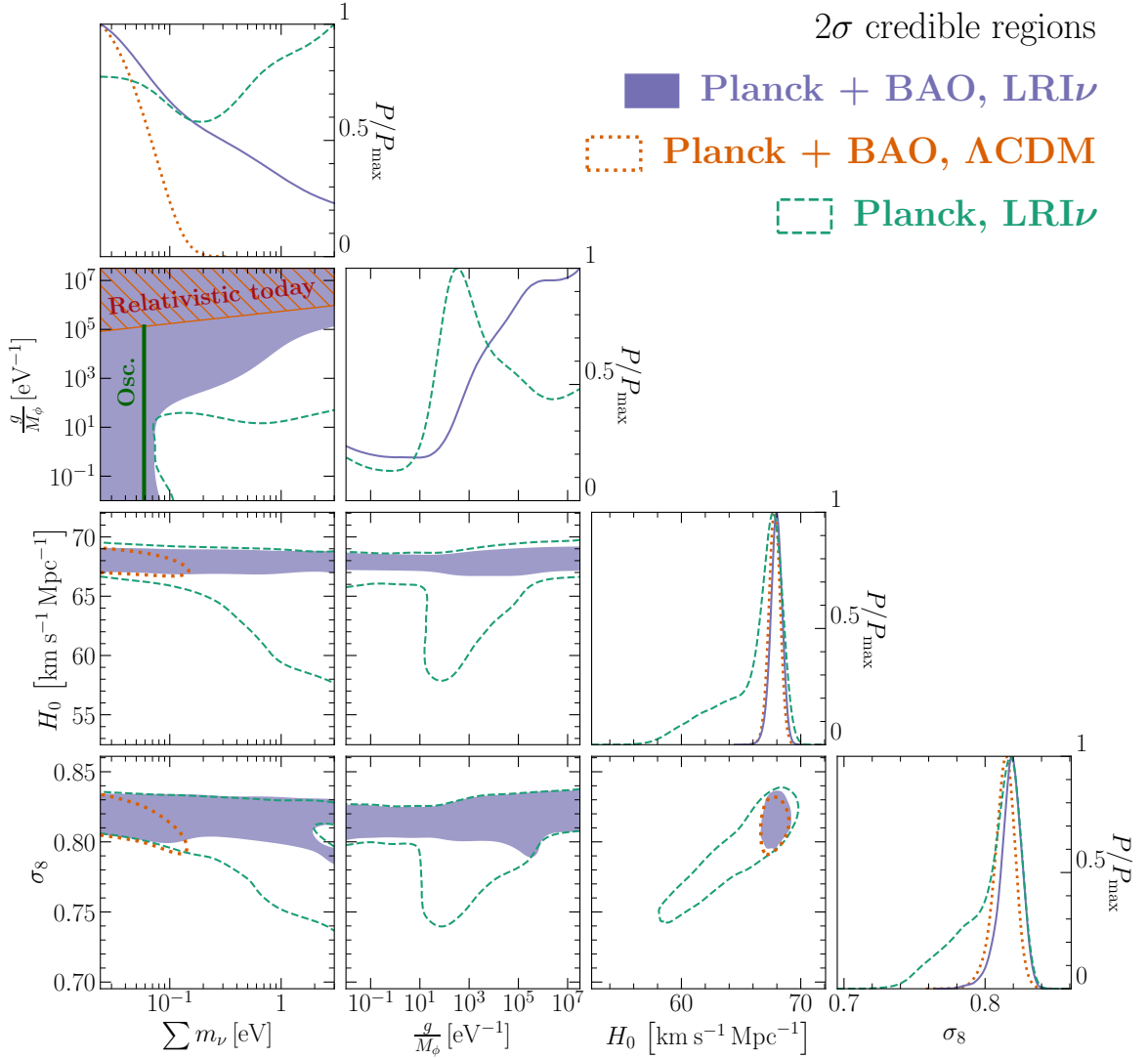


Figure 9: Planck 2018+BAO constraints [78, 113–115] on long range interacting neutrinos, LRI ν , [solid purple], on Λ CDM with non-interacting massive neutrinos [dotted orange], and Planck 2018 constraints [78] on long range interacting neutrinos [dashed green]. We show the marginalized 2σ credible regions and 1-D posterior probability distributions for the most relevant parameters. For $\sum m_\nu$ and $\frac{g}{M_\phi}$, posteriors are constructed with uniform logarithmic bins. In the hatched region, cosmic neutrinos are relativistic today. The solid dark green line is the minimum value of $\sum m_\nu$ allowed by neutrino oscillation data [124–126].

For non-interacting massive neutrinos, we observe the well-known enhancement at $k \sim 10^{-3}h/\text{Mpc}$ and the suppression at large k . The former is due to non-relativistic neutrinos falling in the dark matter gravitational wells and thus contributing to structure growth. The latter is due to the massive neutrino contribution to the energy density of the Universe: massive neutrinos increase the Hubble parameter with respect to the massless scenario (as they have an equation of state $w < 1/3$ and thus redshift slower), which in turn suppresses

range interactions.

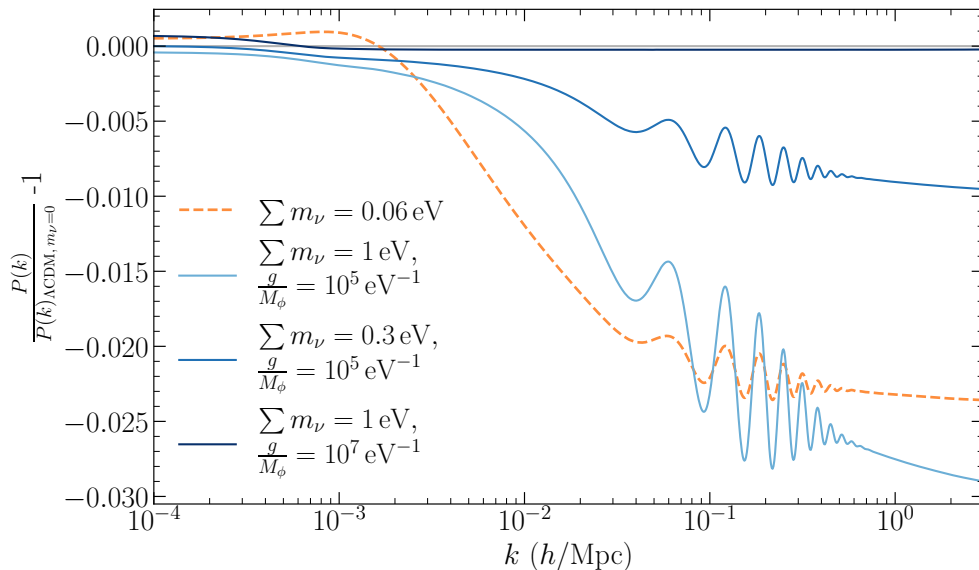


Figure 10: Relative difference in linear matter power spectrum between Λ CDM with massless neutrinos and massive neutrinos with total mass $\sum m_\nu$ and interaction long range strength $\frac{g}{M_\phi}$. The dashed orange line corresponds to non-interacting massive neutrinos with the smallest mass allowed by oscillations, which should be detectable at $\sim 2\sigma$ – 3σ with EUCLID [61, 63]. To generate the curves, we have fixed ω_b , ω_{cdm} , H_0 , A_s , n_s , and τ_{reio} . The non-zero values at low k are within numerical uncertainties.

structure growth. Long range interactions delay the relativistic to non-relativistic transition (see Fig. 2b) and modify the equation of state (see Fig. 5). Therefore, they remove the power spectrum enhancement at $k \sim 10^{-3} h/\text{Mpc}$ and modify the Hubble friction-induced large k suppression. Both effects are visible in the solid blue lines in Fig. 10. The future EUCLID survey should have ~ 2 – 3σ sensitivity to the dashed orange line [61, 63],⁹ and so it could probe the parameters corresponding to the light blue line, allowed by current Planck and BAO data.

To quantitatively explore the potential of EUCLID, we have carried out a Bayesian analysis combining current Planck CMB data with an EUCLID power spectrum and lensing forecast following the prescriptions of Refs. [63, 116]. We have included non-linearities using the HALOFIT semi-analytic prescription [135, 136], but we have not added any theoretical errors associated to them. Therefore, we have chosen a minimum comoving scale $k_{\text{max}} = 0.2 h/\text{Mpc}$ ($0.5 h/\text{Mpc}$) for the power spectrum (lensing) data. This roughly corresponds to the scale at which present-day theoretical errors match the smallest EUCLID observational uncertainties [63], so we don’t expect the future data sensitivity to be very different from our results. Finally, following Ref. [63] (see also Refs. [137–140]), we have only included the baryon and cold dark matter power spectrum in the EUCLID galaxy power spectrum determination.

We show the results of our analysis in Fig. 11. In solid, we show the 1-D posterior probabilities and the marginalized 2-D 2σ credible regions for the sum of neutrino masses $\sum m_\nu$ and the long range interaction strength $\frac{g}{M_\phi}$. In dotted, we show the results from our Planck 2018 + BAO analysis (see Fig. 9). In the hatched region cosmic neutrinos are relativistic today,

⁹Present-day uncertainties on the matter power spectrum are larger than the range in Fig. 10.

and the green line is the minimum value of $\sum m_\nu$ allowed by neutrino oscillation data [124–126]. We have generated EUCLID mock data using the best fit cosmological parameters of the Planck 2018 + BAO Λ CDM analysis [78], no long range interactions, and two values for the sum of neutrino masses as labeled by the captions. On the one hand, the mock data for the analysis results in Fig. 11a has been generated with the smallest neutrino mass allowed by our priors in Table 1. This value is in direct tension with neutrino oscillation measurements and corresponds to EUCLID results compatible with massless neutrinos. On the other hand, in Fig. 11b, we have generated the data with $\sum m_\nu = 0.08$ eV. This value is compatible with present cosmological bounds and is well within the EUCLID sensitivity. For completeness, we show in Appendix C the posterior probabilities and credible regions for all parameters in our analysis.

Figure 11 shows that, as expected, EUCLID data will improve the Planck 2018 + BAO constraints. Depending on the outcome of the EUCLID observations, we can consider two qualitatively distinct scenarios:

- *EUCLID data is consistent with massless neutrinos.* With the projected sensitivity, this would be a contradiction between cosmological observations and neutrino oscillation experiments, and thus a hint for new physics. The resulting prospects for an analysis assuming long range interacting neutrinos are shown in Fig. 11a. As we see, long range interactions could explain the apparent cosmology-oscillations discrepancy for interaction strengths $g/M_\phi \sim 10^2$ – 10^5 eV $^{-1}$.
- *EUCLID data is consistent with massive non-interacting neutrinos.* This is the expected outcome, compatible with no new physics. The observed shape of the power spectrum (see Fig. 10) would exclude neutrino long range interaction strengths $g/M_\phi \gtrsim 10^4$ eV $^{-1}$. Furthermore, even within our model, the measurement of the neutrino mass would be relatively robust, the upper limit being relaxed by $\sim 40\%$ for $g/M_\phi \sim 10^3$ eV $^{-1}$.

Moreover, as mentioned in the previous subsection, a neutrino mass detection at KATRIN of $\sum m_\nu \gtrsim 0.6$ eV could point to long range interactions with strength $g/M_\phi \sim 10^3$ – 10^5 eV $^{-1}$. As we see in Fig. 11, these parameter values can be explored by EUCLID, allowing to test this hypothesis.

4 Summary and Conclusions

In this work, we have consistently explored the cosmology of fermions endowed with a scalar-mediated long range interaction. We have then applied the general formalism to the particular case of self-interacting neutrinos, for which we have performed an analysis of current and near future cosmological data.

We have started by obtaining the evolution equations in Section 2. We have focused on long range effects on the energy density and equation of state of the fermion system, that directly impact the cosmological evolution. For this, we have studied the regime where the effective scalar mass M_{eff} (2.18) is much larger than the Hubble parameter and collisions among fermions can be neglected. Relaxing the first assumption would recover quintessence and modified gravity-like scenarios, whereas relaxing the second assumption would introduce additional particle creation, annihilation and momentum transfer processes. Both limits have been widely studied in the literature [6–13, 21, 22, 30–36, 91–98].

To solve the evolution of the system, we have chosen as our initial conditions a Fermi-Dirac momentum distribution for the fermions, as well as no initial scalar field except for the

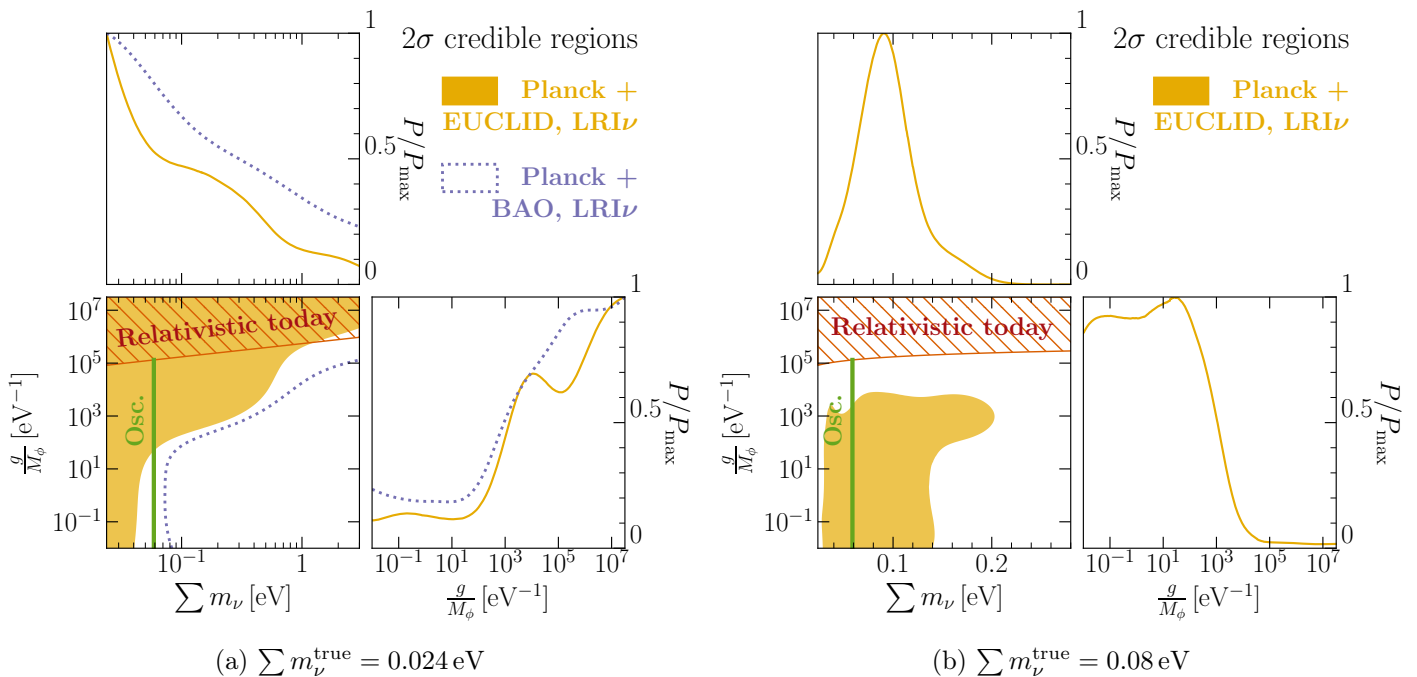


Figure 11: Future EUCLID + Planck 2018 constraints [60, 63, 78] on long range interacting neutrinos, LRI ν , [solid yellow], and Planck 2018 + BAO constraints [78, 113–115] [dotted purple]. We show the marginalized 2σ credible regions and 1-D posterior probability distributions for $\sum m_\nu$ and $\frac{g}{M_\phi}$. In the left panel, posteriors are constructed with uniform logarithmic bins. In the right panel, only the posterior on $\frac{g}{M_\phi}$ is constructed with logarithmic bins, and the prior on $\sum m_\nu$ is taken to be linear. In the hatched region, cosmic neutrinos are relativistic today; and the green line is the minimum total neutrino mass allowed by oscillation data [124–126]. We have generated EUCLID mock data with the best fit parameters from the Λ CDM Planck 2018 + BAO analysis (last column in Table 2 in Ref. [78]), no long range interactions and two different values of the total neutrino mass $\sum m_\nu^{\text{true}}$: 0.024 eV [left], the smallest value compatible with our priors, and consistent with massless neutrinos within EUCLID precision; and 0.08 eV [right], a value compatible with CMB and BAO data that should be well-measurable by EUCLID.

one sourced by the fermions. Our main results are Figs. 2 and 5, where we show the total energy density and equation of state of the system as well as the effective fermion mass as a function of the fermion temperature T . We have found that long range effects turn on for T below the vacuum fermion mass m_0 , and they are relevant if $\frac{gm_0}{M_\phi} > 1$. In other words, if for $T < m_0$ the interparticle distance is smaller than the interaction range.

As the Universe expands and the fermion temperature decreases, we have obtained that the fermion system first behaves as radiation even for temperatures well below m_0 , as the sourced scalar field reduces the effective fermion mass. Later on, the scalar field energy density takes over and the equation of state parameter w can take negative values. Finally, when the system cools down and the interparticle distance gets larger than the interaction range, fermions become effectively non-relativistic. At this point, the long range interaction is generically much stronger than gravity and fermion perturbations collapse in very short

timescales $\sim M_{\text{eff}}^{-1} \ll H^{-1}$, forming non-linear structures or *nuggets* with typical sizes $\lesssim M_{\text{eff}}^{-1}$ outside which no scalar field is left. Supported by analytic estimations, we have chosen to model this collapse as an *instantaneous* transition to a dust-like behavior.

In Section 3, we have confronted these new interactions with data, focusing on long range interactions among neutrinos. We have discussed the consequences on CMB, BAO and LSS observables (Figs. 6, 8 and 10), as well as their physical origin. For this, we have modified the CLASS code to include long range interacting fermions. Our modification is publicly available [at this URL](#) . We have also performed a Bayesian analysis to present Planck 2018 and BAO data (Figs. 7 and 9). We have obtained that the cosmological neutrino mass bound is completely removed once long range interactions are included, due to the effective neutrino mass induced by the scalar field. Thus, in our simple modification the KATRIN experiment could detect neutrino masses ~ 1 eV as long as the self interaction strength is $g/M_\phi \sim 10^3\text{--}10^6$ eV $^{-1}$.

We have also concluded that BAO data plays an important role in breaking degeneracies. This is mostly due to BAO being a late-time cosmological probe, as neutrinos become non-relativistic relatively late. Because of this, we expect next generation LSS data to efficiently explore long range neutrino self interactions. In Section 3.2, we have carried out a forecast of the future EUCLID survey (Fig. 11), that aims to be sensitive enough to detect the smallest neutrino mass allowed by oscillations. Nevertheless, if EUCLID observations are compatible with massless neutrinos, we have found that long range interactions could explain the apparent discrepancy with oscillation experiments. If, in turn, EUCLID results are compatible with massive, non-interacting neutrinos, the long range interaction strength would be constrained to be $g/M_\phi \lesssim 10^4$ eV $^{-1}$. In this scenario, a positive mass measurement would be quite robust against the presence of long range interactions, though the upper limit on the neutrino mass would be relaxed for $g/M_\phi \sim 10^3$ eV $^{-1}$. Finally, if KATRIN measures a non-zero neutrino mass, EUCLID could test whether the apparent discrepancy between KATRIN and CMB and BAO data is due to long range interactions.

In summary, in this work we have seen that long range interactions can dramatically alter the equation of state of cosmological systems. By dropping the ideal gas assumption, interacting fermion systems might behave as ultrarelativistic at relatively low temperatures or even as dark energy. For the case of neutrinos, cosmological probes sensitively explore this physics, at the same time affecting the neutrino mass bound. This opens the possibility for a laboratory detection of the neutrino mass scale in the near future.

Acknowledgments

We would like to thank M. C. Gonzalez-Garcia for very helpful comments and discussions and a careful reading of the manuscript, Alessio Notari for early discussions, and John Beacom for comments. This work has been funded by the European ITN project H2020-MSCA-ITN-2019/860881-HIDDeN, the Spanish grants FPA2016-76005-C2-1-P, PID2019-108122GB-C32, PID2019-105614GB-C21. IE acknowledges support from the FPU program fellowship FPU15/03697, and warmly thanks CCAPP for their valuable support and hospitality during the final stages of this work.

A Classical Limit of the Evolution Equations

The evolution of the fermion and scalar field is dictated by the quantum evolution equations Eqs. (2.2) and (2.3). In this Appendix, we will obtain the classical limit relevant for the cosmological scales we are interested in.

As discussed in Section 2, we will analyze our system in terms of a phase space distribution $f(x^\mu, P_\mu)$ of fermions with positions x^μ and conjugate momenta P_μ , and a classical scalar field $\phi(x^\mu)$. In the classical limit, all quantum operators \hat{O} can be replaced by their expectation values

$$\langle \hat{O} \rangle \equiv \sum_s \int \frac{dP_1 dP_2 dP_3}{\sqrt{-\mathcal{G}}} \frac{1}{2P^0} f(x^\mu, P_\mu, s) \langle \phi, P^s | \hat{O} | \phi, P^s \rangle, \quad (\text{A.1})$$

where

- $P_i = \tilde{m} \frac{dx_i}{d\lambda}$ is the conjugate momentum to the position x^i of the fermions, with $\tilde{m} \equiv \sqrt{-P_\mu P^\mu}$ their mass and λ their proper time.
- \mathcal{G} is the metric determinant.
- s is the fermion spin.
- $|\phi, P^s\rangle \equiv |\phi\rangle \otimes |P^s\rangle$, with $|\phi\rangle$ a state with classical scalar field ϕ and $|P^s\rangle$ a one-particle fermion state with momentum P and spin s . The former can be described by a coherent state [141–143]

$$|\phi\rangle \equiv e^{-\frac{1}{2} \int \frac{d^3K}{(2\pi)^3} \frac{|\phi(K)|^2}{(2K^0)^5}} e^{\int \frac{d^3K}{(2\pi)^3} \frac{\phi(K)}{(2K^0)^{5/2}} a_K^\dagger} |0\rangle, \quad (\text{A.2})$$

where

- $\phi(K)$ is the Fourier transform of the classical scalar field $\phi(x)$, i.e.,

$$\phi(x) \equiv \int \frac{d^3K}{(2\pi)^3} \frac{1}{(\sqrt{2}K^0)^3} [\phi(K)e^{-iKx} + \phi(K)^*e^{iKx}]. \quad (\text{A.3})$$

- a_K^\dagger is an annihilation operator of the field $\hat{\phi}$ with momentum K .
- $|0\rangle$ is the vacuum.

The fermion one-particle state is given by [144]

$$|P^s\rangle \equiv \sqrt{2P^0} a_P^{s\dagger} |0\rangle, \quad (\text{A.4})$$

where a_P^s is an annihilation operator of the field ψ with momentum P .

We first start with the classical limit of Eq. (2.3). For convenience, we Fourier-expand the fermion field ψ in terms of creation and annihilation operators following the conventions of Ref. [144], and Eq. (2.3) reads¹⁰

$$a_P^s \left[\gamma_\mu P^\mu u^s(P) + (m_0 + g\hat{\phi})u^s(P) \right] = 0, \quad (\text{A.5})$$

$$b_P^{s\dagger} \left[\gamma_\mu P^\mu v^s(P) - (m_0 + g\hat{\phi})v^s(P) \right] = 0, \quad (\text{A.6})$$

¹⁰We are also implicitly assuming that $\phi(x^\mu)$ can be considered to be constant inside the coherence length of the fermion field Ψ .

with b_P^s an antifermion annihilation operator and $\{u^s, v^s\}$ the spinor solutions to the Dirac equation. If we multiply Eq. (A.5) by $a_P^{s\dagger} \left[u^{s\dagger}(P) \gamma_\mu P^\mu - (m_0 + g\hat{\phi}) u^{s\dagger}(P) \right]$, and the Hermitian conjugate of Eq. (A.6) by $b_P^{s\dagger} \left[\gamma_\mu^\dagger P^\mu v^s(P) + (m_0 + g\hat{\phi}) v^{s\dagger}(P) \right]$, we get

$$a_P^{s\dagger} a_P^s u^{s\dagger}(P) u^s(P) \left[-\tilde{m}^2 + (m_0 + g\hat{\phi})^2 \right] = 0, \quad (\text{A.7})$$

$$b_P^{s\dagger} b_P^s v^{s\dagger}(P) v^s(P) \left[-\tilde{m}^2 + (m_0 + g\hat{\phi})^2 \right] = 0. \quad (\text{A.8})$$

We can now take classical expectation values using Eq. (A.1). Since $\langle \phi | \phi \rangle = 1$ and $\langle \phi | \hat{\phi} | \phi \rangle = \phi$, the Dirac equations simply read

$$-\tilde{m}^2 + (m_0 + g\phi)^2 = 0, \quad (\text{A.9})$$

and so we have obtained the effective fermion mass

$$\tilde{m} = m_0 + g\phi. \quad (\text{A.10})$$

Finally, we can also take the expectation value of the scalar field equation (2.2),

$$-D_\mu D^\mu \phi + M^2 \phi = -g \sum_s \int \frac{dP_1 dP_2 dP_3}{\sqrt{-\mathcal{G}}} \frac{1}{2P^0} f(x^\mu, P_\mu, s) \langle P^s | \bar{\psi} \psi | P^s \rangle. \quad (\text{A.11})$$

The expectation value on the right-hand side can be immediately evaluated

$$\langle P^s | \bar{\psi} \psi | P^s \rangle = \bar{u}^s(P) u^s(P) = 2\tilde{m}. \quad (\text{A.12})$$

The same final result would be obtained if our state also contained antifermions. Thus, our final equation for the scalar field reads

$$-D_\mu D^\mu \phi + M^2 \phi = -g \int \frac{dP_1 dP_2 dP_3}{\sqrt{-\mathcal{G}}} \frac{\tilde{m}}{P^0} f(x^\mu, P_\mu), \quad (\text{A.13})$$

where fermions, antifermions, and all spin orientations equally contribute to f .

To obtain the energy density and pressure of the system, we can compute the expectation value of the stress-energy tensor using Eqs. (2.1) and (A.1). The homogeneous and isotropic results correspond to Eqs. (2.22) and (2.23).

B Properties of the Adiabatic Instability

As discussed in Section 2.2, non-relativistic fermion density perturbations can grow exponentially under the presence of long range scalar interactions. In this Appendix, we will approximately compute the fermion temperatures and interaction strengths for which this instability is present. We will also estimate the timescale over which non-linear *nugget* formation takes place, and the conditions under which this happens much faster than cosmological scales. We will mostly follow the methodology in Ref. [102].

From now on, we will assume that the adiabatic approximation (2.38) always holds. As discussed in Section 2.2, this means that the inverse scalar effective mass $\left[(k/a)^2 + M_\phi^2 + M_T^2 \right]^{-1/2}$ is much smaller than other timescales in the perturbed Klein Gordon equation (2.37). These timescales are

- The Hubble scale, H^{-1} , which controls both the Hubble friction term as well as the timescale over which the background quantities \tilde{m} and ε change.
- The timescale over which Ψ_0 changes. We will later check that this scale is $\gtrsim k/a$.

Since we are already assuming $M_\phi^2 + M_T^2 \gg H^2$ (see Section 2.1.1), the adiabatic approximation holds as long as $M^2 + M_T^2 \gg (k/a)^2$. In other words, we will solve the perturbation equations for physical length scales a/k much larger than the interaction range. In addition, we will neglect metric perturbations in the Boltzmann equation (2.32). Using Eq. (2.38), this equation then reads

$$\frac{\partial \Psi(\vec{q}, \vec{k}, \tau)}{\partial \tau} + i \frac{\vec{k} \cdot \vec{q}}{\varepsilon(\tau)} \Psi(\vec{q}, \vec{k}, \tau) + i \frac{\vec{k} \cdot \vec{q}}{\varepsilon(\tau)} \tilde{m}(\tau) \frac{d \log f_0}{d \log q} \frac{g^2 \int d^3 q \frac{\tilde{m}(\tau)}{\varepsilon(\tau)} f_0(q) \Psi(\vec{q}, \vec{k}, \tau)}{(k/a)^2 + M_\phi^2 + M_T^2} = 0, \quad (\text{B.1})$$

where $\vec{q} \equiv q\hat{n}$. This first order integro-differential equation cannot be solved in general. If, however, we consider timescales that are short with respect to cosmological evolution, the functions $\tilde{m}(\tau)$, $\varepsilon(\tau)$ and $M_T(\tau)$ can be assumed to be constant. We can then Fourier-transform in time

$$\Psi(\vec{q}, \vec{k}, \tau) = \int d\omega \tilde{\Psi}(\vec{q}, \vec{k}, \omega) e^{-i\omega\tau}, \quad (\text{B.2})$$

and the equation reads

$$-\omega \tilde{\Psi}(\vec{q}, \vec{k}, \omega) + \frac{\vec{k} \cdot \vec{q}}{\varepsilon} \tilde{\Psi}(\vec{q}, \vec{k}, \omega) + \frac{\vec{k} \cdot \vec{q}}{\varepsilon} \tilde{m} \frac{d \log f_0}{d \log q} \frac{g^2 \int d^3 q \frac{\tilde{m}}{\varepsilon} f_0(q) \tilde{\Psi}(\vec{q}, \vec{k}, \omega)}{(k/a)^2 + M_\phi^2 + M_T^2} = 0, \quad (\text{B.3})$$

or, rearranging terms,

$$\tilde{\Psi}(\vec{q}, \vec{k}, \omega) = \left[\int d^3 q \frac{\tilde{m}^2}{\varepsilon} f_0(q) \tilde{\Psi}(\vec{q}, \vec{k}, \omega) \right] \frac{-g^2 \frac{\vec{k} \cdot \vec{q}}{q^2 \varepsilon} \frac{d \log f_0}{d \log q}}{\left(-\omega + \frac{\vec{k} \cdot \vec{q}}{\varepsilon}\right) \left(k^2/a^2 + M_\phi^2 + M_T^2\right)}. \quad (\text{B.4})$$

To remove the dependence on $\tilde{\Psi}$, we multiply both sides by $\frac{\tilde{m}^2}{\varepsilon} f_0(q)$ and integrate over \vec{q} . Writing $d^3 q = 2\pi q^2 dq d(\vec{q} \cdot \vec{k})/k$, we can perform the angular integral and then integrate by parts, getting in the end

$$\frac{(k/a)^2 + M_\phi^2 + M_T^2}{g^2 \tilde{m}^2} = 4\pi \int_0^\infty dq \frac{q^2 \tilde{m}^2}{\varepsilon^3 \left[q^2 - \frac{\omega^2}{k^2} \varepsilon^2\right]} f_0(q), \quad (\text{B.5})$$

an equation that gives $\omega = \omega(k, \frac{gm_0}{M_\phi}, T/M_0)$. Linear perturbations will be unstable if (and only if) this equation admits solutions with imaginary ω .

We will first study the existence of unstable solutions. As, for imaginary ω , the right-hand side of Eq. (B.5) is a monotonically growing function of ω^2 , there will be no unstable solutions if the left-hand side is greater than the right-hand side evaluated at $\omega^2 = 0$. That is, the system is unstable if and only if

$$\frac{(k/a)^2 + M_\phi^2 + M_T^2}{g^2 \tilde{m}^2} \leq 4\pi \int_0^\infty dq \frac{\tilde{m}^2}{\varepsilon^3} f_0(q). \quad (\text{B.6})$$

This equation is quite instructive to understand the differences between this instability and the familiar Jeans gravitational instability. First, for ultrarelativistic fermions $\varepsilon \gg \tilde{m}$, the

right-hand side will be suppressed, and the system will generically be stable. That is, relativistic random thermal motions stabilize perturbations at all scales for scalar self interactions. This is different to the case of gravity, which has an infinite range (corresponding to $M_\phi^2 + M_T^2 \rightarrow 0$ in Eq. (B.6)) and thus for low enough k there is always a scale, the Jeans scale, above which the accumulated gravitational attraction overcomes random thermal motions and perturbations collapse. Turning back to the scalar self interaction, even in the non-relativistic limit, for low enough fermion number densities the right-hand side of Eq. (B.6) decreases and the system is again stable. Physically, for interparticle distances larger than the interaction range scalar interactions turn off. Again, this is not the case for an infinite-range interaction as gravity, where the left-hand side of Eq. (B.6) can be made arbitrarily small by considering arbitrarily large scales.

In order to obtain the temperatures and interaction strengths at which the system is unstable, we have numerically solved Eq. (B.6) in the limit $M_\phi^2 + M_T^2 \gg (k/a)^2$ (as discussed at the beginning of this Appendix) for the Fermi-Dirac fermion distribution function in Eq. (2.21). Our results are in shaded in Fig. 4, where the blank region for which the system is stable corresponds to the two physical scenarios discussed above.

Apart from computing the temperatures and interaction strengths for which the system is unstable, Eq. (B.5) also allows to estimate the timescale ω over which fermion density perturbations become non-linear and collapse in *nuggets* as discussed in Section 2.2. To this purpose, we have numerically solved Eq. (B.5) to obtain $(\omega/k)^2$ in the limit $M^2 + M_T^2 \gg (k/a)^2$ (as discussed at the beginning of this Appendix) and for the Fermi-Dirac fermion distribution function in Eq. (2.21). We show in Fig. 12 $(\omega/k)^2$ as a function of the fermion temperature (normalized to its effective mass) for different interaction strengths $\frac{gm_0}{M_\phi}$. As we see, as soon as the system is unstable, $|\omega/k|$ quickly becomes $\mathcal{O}(1)$.

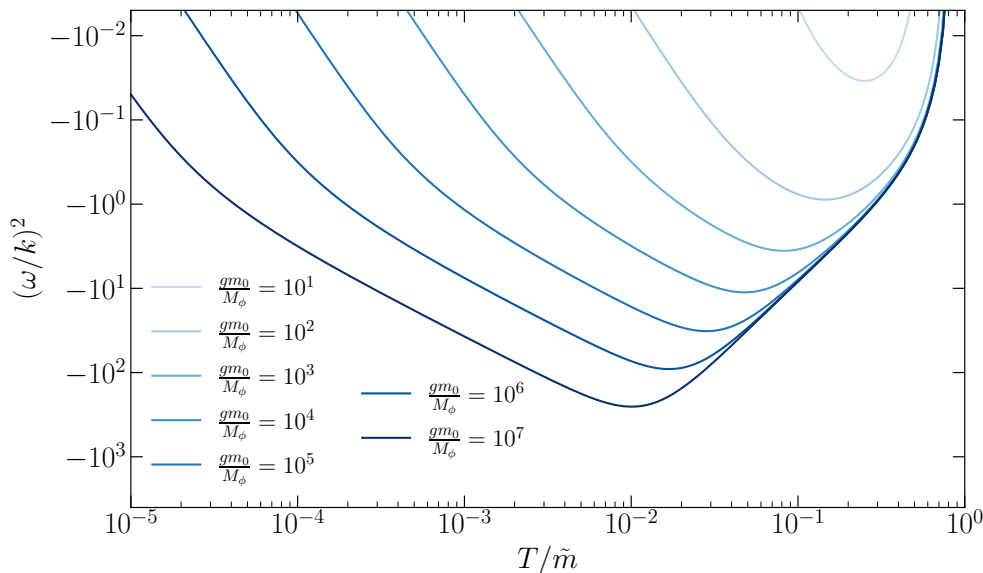


Figure 12: Perturbation growth rate as measured by $(\omega/k)^2$ as a function of T/\tilde{m} for different interaction strengths [solid blue shades]. The curves cross $\omega/k = 0$ at the temperature of instability onset.

Nevertheless, under the assumptions in this Appendix, we can only compute perturba-

tion growth for small timescales $\delta\tau$ during which all functions in Eq. (B.1) except for Ψ can be considered to be constant. Over these timescales, unstable perturbations grow by a factor $e^{|\omega|\delta\tau}$. Since the initial perturbations are $\sim 10^{-4}$ – 10^{-5} , we will consider that fermion *nuggets* form if

$$|\omega|\delta\tau > \log(10^4\text{--}10^5) \gtrsim 10. \quad (\text{B.7})$$

In this case, *nuggets* will form instantly with respect to cosmological time, and the instability can be modeled as an instantaneous transition to a dust-like behavior. A plausible value for $\delta\tau$ can be estimated as follows: if $\omega(\tau)$ as computed from Eq. (B.5) is constant, then all relevant parameters in that equation are also constant. We have thus taken $\delta\tau$ as a fraction ε of the typical time during which $\omega(\tau)$ changes

$$\delta\tau = \varepsilon \left| \frac{\omega}{d\omega/d\tau} \right|, \quad (\text{B.8})$$

where $d\omega/d\tau$ can be obtained from Fig. 12. By conservatively assuming $\varepsilon = 10^{-2}$ and $k/a = 0.1\sqrt{M_\phi^2 + M_T^2}$, our condition (B.7) for instantaneous nugget formation is equivalent to

$$\sqrt{M_\phi^2 + M_T^2} \gtrsim 10^5 H, \quad (\text{B.9})$$

at instability onset. This corresponds to Eq. (2.39) in the main text.

C Statistical Analysis in the Whole Parameter Space

In this Appendix, we show the results of our Bayesian analysis (Figs. 7, 9 and 11) for all cosmological parameters. Figure 13 corresponds to the analysis of Planck 2018 data, Fig. 14 also includes BAO data, and Figs. 15 and 16 corresponds to the analysis prospects of EUCLID and Planck 2018 data. See the main text for the description of the analysis.

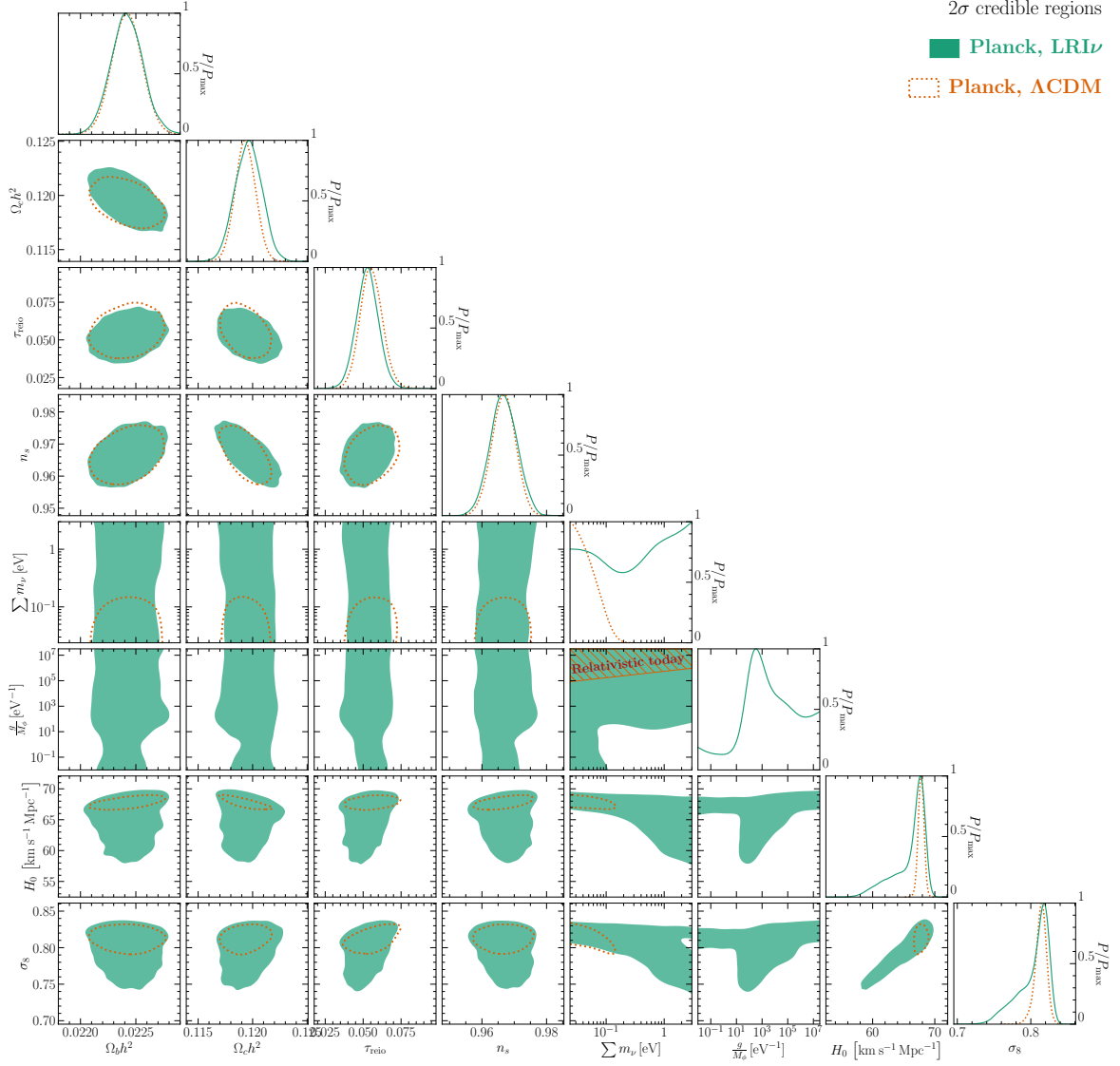


Figure 13: Planck 2018 constraints [78] on neutrino long range interactions [solid light green] and on Λ CDM with non-interacting massive neutrinos [dotted orange]. We show the marginalized 2σ credible regions and 1-D posterior probability distributions. For $\sum m_\nu$ and $\frac{g}{M_\phi}$, posteriors are constructed with uniform logarithmic bins. In the hatched region, cosmic neutrinos are relativistic today. The dark green line is the minimum value of $\sum m_\nu$ allowed by neutrino oscillation data [124–126].

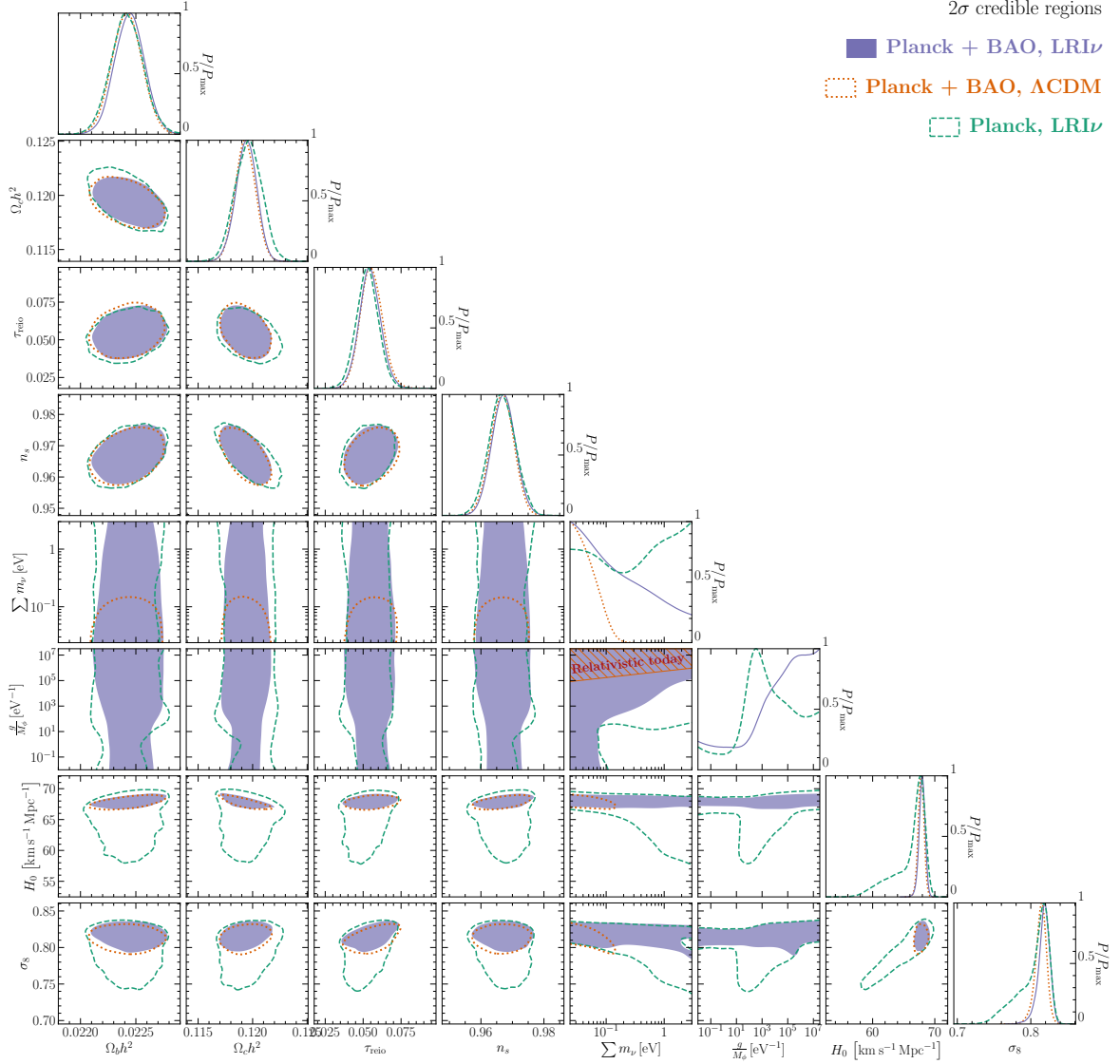


Figure 14: Planck 2018+BAO constraints [78, 113–115] on neutrino long range interactions [solid purple], on Λ CDM with non-interacting massive neutrinos [dotted orange], and Planck 2018 constraints [78] on neutrino long range interactions [dashed green]. We show the marginalized 2σ credible regions and 1-D posterior probability distributions. For $\sum m_\nu$ and $\frac{g}{M_\phi}$, posteriors are constructed with uniform logarithmic bins. In the hatched region, cosmic neutrinos are relativistic today. The solid dark green line is the minimum value of $\sum m_\nu$ allowed by neutrino oscillation data [124–126].

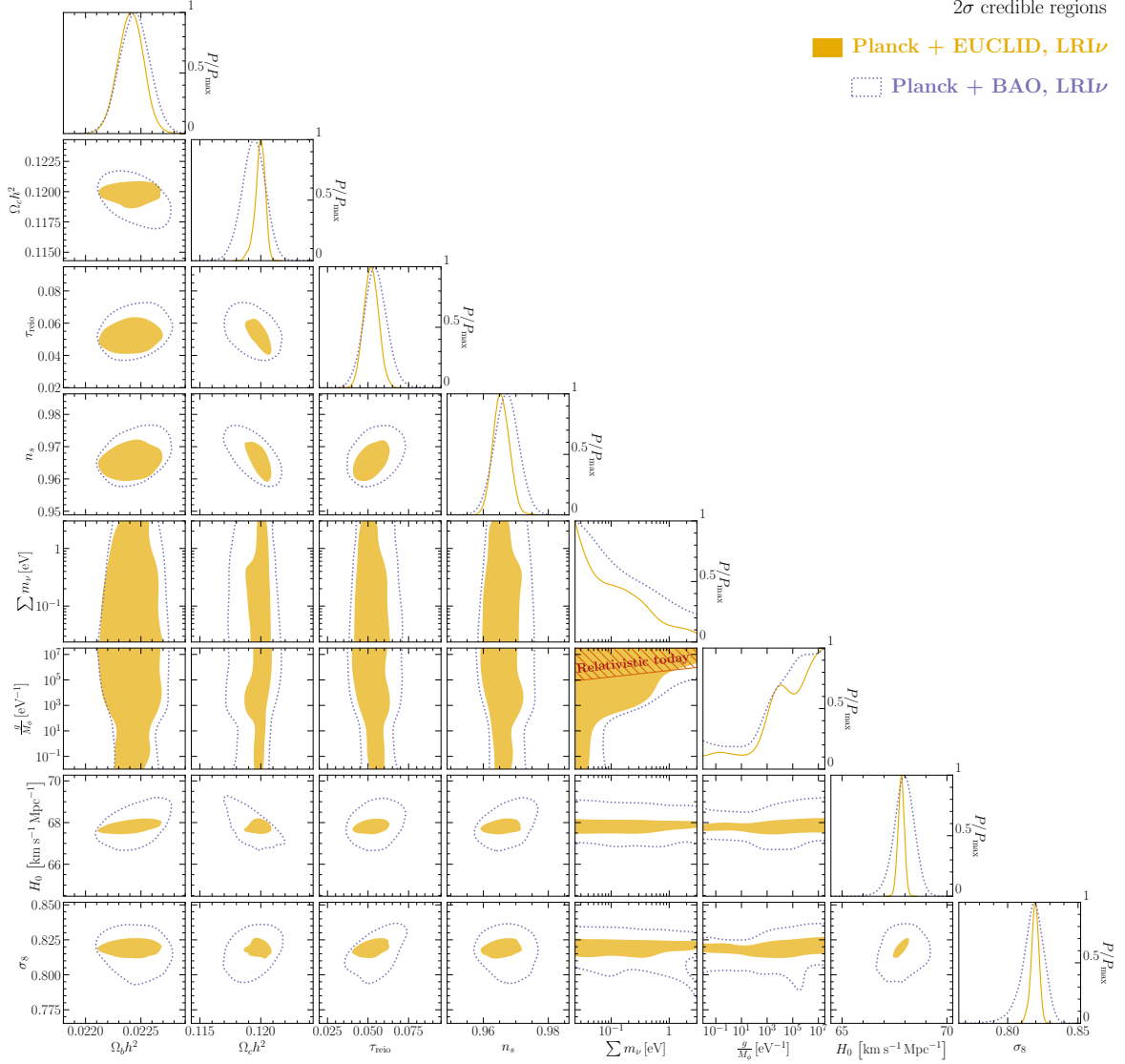


Figure 15: Future EUCLID + Planck 2018 constraints [60, 63, 78] on long range interacting neutrinos, LRI ν , [solid yellow], and Planck 2018 + BAO constraints [78, 113–115] [dotted purple]. We show the marginalized 2 σ credible regions and 1-D posterior probability distributions. For $\sum m_\nu$ and $\frac{g}{M_\phi}$, posteriors are constructed with uniform logarithmic bins. In the hatched region, cosmic neutrinos are relativistic today. We have generated EUCLID mock data with the best fit parameters from the Λ CDM Planck 2018 + BAO analysis (last column in Table 2 in Ref. [78]), no long range interactions and $\sum m_\nu = 0.024$ eV, the smallest value compatible with our priors, and consistent with massless neutrinos within EUCLID precision.

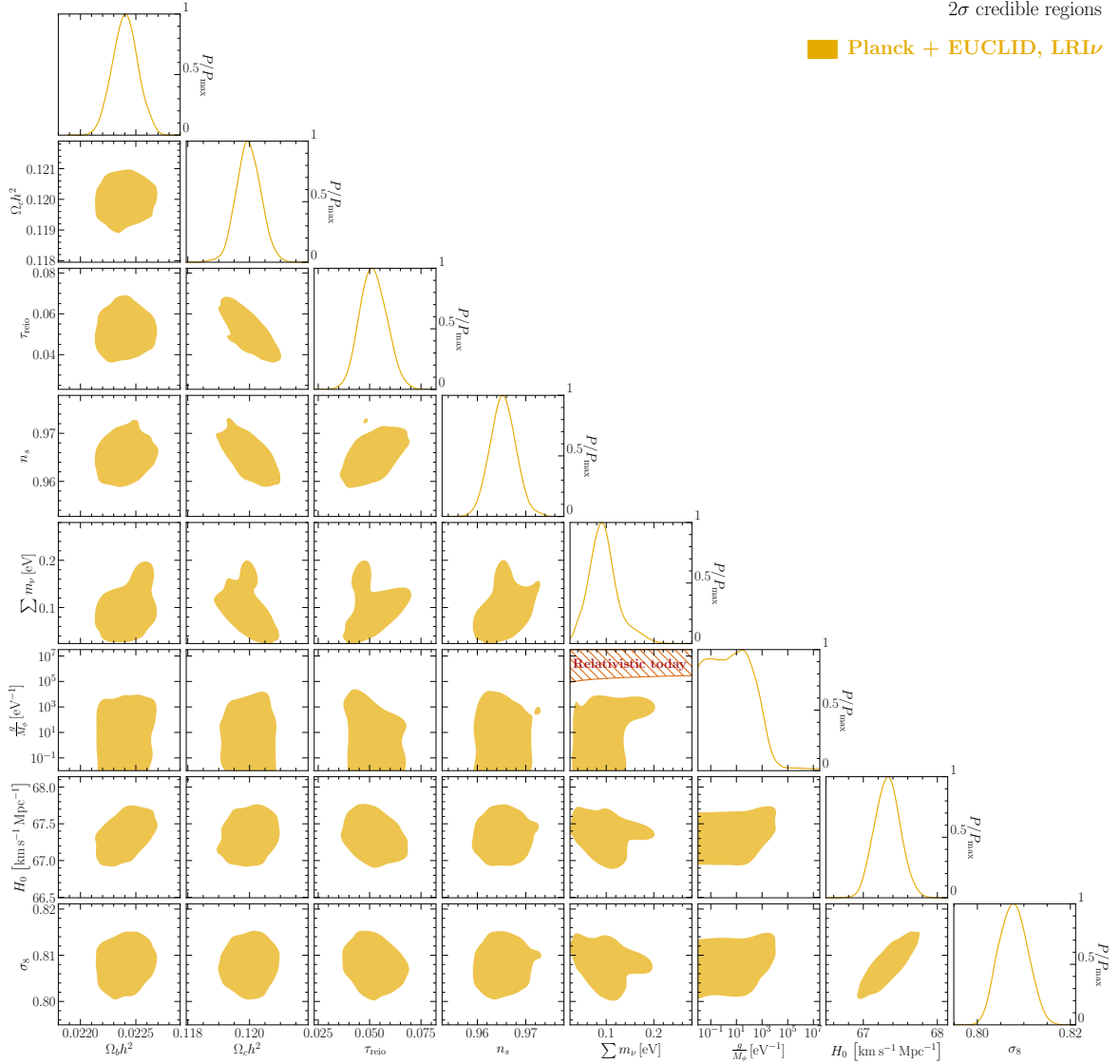


Figure 16: Future EUCLID + Planck 2018 constraints [60, 63, 78] on long range interacting neutrinos, LRI ν , [solid yellow]. We show the marginalized 2 σ credible regions and 1-D posterior probability distributions. For $\frac{g}{M_\phi}$, posteriors are constructed with uniform logarithmic bins. The prior on $\sum m_\nu$ is taken to be linear. In the hatched region, cosmic neutrinos are relativistic today. We have generated EUCLID mock data with the best fit parameters from the Λ CDM Planck 2018 + BAO analysis (last column in Table 2 in Ref. [78]), no long range interactions and $\sum m_\nu = 0.08$ eV, a value compatible with CMB and BAO data that should be well-measurable by EUCLID.

References

- [1] E. Fischbach and C. Talmadge, *Ten years of the fifth force*, in *31st Rencontres de Moriond: Dark Matter and Cosmology, Quantum Measurements and Experimental Gravitation*, pp. 443–451, 1996, [hep-ph/9606249](#).
- [2] E. Adelberger, B. R. Heckel and A. Nelson, *Tests of the gravitational inverse square law*, *Ann. Rev. Nucl. Part. Sci.* **53** (2003) 77 [[hep-ph/0307284](#)].
- [3] J. G. Williams, S. G. Turyshev and D. H. Boggs, *Progress in lunar laser ranging tests of relativistic gravity*, *Phys. Rev. Lett.* **93** (2004) 261101 [[gr-qc/0411113](#)].
- [4] E. Adelberger, J. Gundlach, B. Heckel, S. Hoedl and S. Schlamminger, *Torsion balance experiments: A low-energy frontier of particle physics*, *Prog. Part. Nucl. Phys.* **62** (2009) 102.
- [5] T. Wagner, S. Schlamminger, J. Gundlach and E. Adelberger, *Torsion-balance tests of the weak equivalence principle*, *Class. Quant. Grav.* **29** (2012) 184002 [[1207.2442](#)].
- [6] J. A. Frieman and B.-A. Gradwohl, *Dark matter and the equivalence principle*, *Phys. Rev. Lett.* **67** (1991) 2926.
- [7] R. Bean, *Perturbation evolution with a nonminimally coupled scalar field*, *Phys. Rev. D* **64** (2001) 123516 [[astro-ph/0104464](#)].
- [8] S. S. Gubser and P. Peebles, *Structure formation in a string inspired modification of the cold dark matter model*, *Phys. Rev. D* **70** (2004) 123510 [[hep-th/0402225](#)].
- [9] A. Nusser, S. S. Gubser and P. Peebles, *Structure formation with a long-range scalar dark matter interaction*, *Phys. Rev. D* **71** (2005) 083505 [[astro-ph/0412586](#)].
- [10] R. Bean, E. E. Flanagan, I. Laszlo and M. Trodden, *Constraining Interactions in Cosmology’s Dark Sector*, *Phys. Rev. D* **78** (2008) 123514 [[0808.1105](#)].
- [11] M. Kesden and M. Kamionkowski, *Galilean Equivalence for Galactic Dark Matter*, *Phys. Rev. Lett.* **97** (2006) 131303 [[astro-ph/0606566](#)].
- [12] Y. Bai, J. Salvado and B. A. Stefanek, *Cosmological Constraints on the Gravitational Interactions of Matter and Dark Matter*, *JCAP* **10** (2015) 029 [[1505.04789](#)].
- [13] N. Mohapi, A. Hees and J. Larena, *Test of the Equivalence Principle in the Dark Sector on Galactic Scales*, *JCAP* **03** (2016) 032 [[1510.06198](#)].
- [14] P. Zhang, M. Liguori, R. Bean and S. Dodelson, *Probing Gravity at Cosmological Scales by Measurements which Test the Relationship between Gravitational Lensing and Matter Overdensity*, *Phys. Rev. Lett.* **99** (2007) 141302 [[0704.1932](#)].
- [15] L. Amendola, M. Kunz and D. Sapone, *Measuring the dark side (with weak lensing)*, *JCAP* **04** (2008) 013 [[0704.2421](#)].
- [16] A. Avilez and C. Skordis, *Cosmological constraints on Brans-Dicke theory*, *Phys. Rev. Lett.* **113** (2014) 011101 [[1303.4330](#)].
- [17] Y.-C. Li, F.-Q. Wu and X. Chen, *Constraints on the Brans-Dicke gravity theory with the Planck data*, *Phys. Rev. D* **88** (2013) 084053 [[1305.0055](#)].
- [18] C. Umiltà, M. Ballardini, F. Finelli and D. Paoletti, *CMB and BAO constraints for an induced gravity dark energy model with a quartic potential*, *JCAP* **08** (2015) 017 [[1507.00718](#)].
- [19] V. Acquaviva and L. Verde, *Observational signatures of Jordan-Brans-Dicke theories of gravity*, *JCAP* **12** (2007) 001 [[0709.0082](#)].
- [20] D. Alonso, E. Bellini, P. G. Ferreira and M. Zumalacárregui, *Observational future of cosmological scalar-tensor theories*, *Phys. Rev. D* **95** (2017) 063502 [[1610.09290](#)].

- [21] J. Solà Peracaula, A. Gomez-Valent, J. de Cruz Pérez and C. Moreno-Pulido, *Brans–Dicke Gravity with a Cosmological Constant Smooths Out Λ CDM Tensions*, *Astrophys. J. Lett.* **886** (2019) L6 [[1909.02554](#)].
- [22] J. Solà Peracaula, A. Gómez-Valent, J. de Cruz Pérez and C. Moreno-Pulido, *Brans–Dicke cosmology with a Λ -term: a possible solution to Λ CDM tensions*, *Class. Quant. Grav.* **37** (2020) 245003 [[2006.04273](#)].
- [23] A. Lessa and O. Peres, *Revising limits on neutrino-Majoron couplings*, *Phys. Rev. D* **75** (2007) 094001 [[hep-ph/0701068](#)].
- [24] P. S. Pasquini and O. L. G. Peres, *Bounds on Neutrino-Scalar Yukawa Coupling*, *Phys. Rev. D* **93** (2016) 053007 [[1511.01811](#)]. [Erratum: *Phys.Rev.D* 93, 079902 (2016)].
- [25] N. Blinov, K. J. Kelly, G. Z. Krnjaic and S. D. McDermott, *Constraining the Self-Interacting Neutrino Interpretation of the Hubble Tension*, *Phys. Rev. Lett.* **123** (2019) 191102 [[1905.02727](#)].
- [26] M. Agostini et al., *Results on $\beta\beta$ decay with emission of two neutrinos or Majorons in ^{76}Ge from GERDA Phase I*, *Eur. Phys. J. C* **75** (2015) 416 [[1501.02345](#)].
- [27] K. Blum, Y. Nir and M. Shavit, *Neutrinoless double-beta decay with massive scalar emission*, *Phys. Lett. B* **785** (2018) 354 [[1802.08019](#)].
- [28] T. Brune and H. Päs, *Massive Majorons and constraints on the Majoron-neutrino coupling*, *Phys. Rev. D* **99** (2019) 096005 [[1808.08158](#)].
- [29] V. Brdar, M. Lindner, S. Vogl and X.-J. Xu, *Revisiting neutrino self-interaction constraints from Z and τ decays*, *Phys. Rev. D* **101** (2020) 115001 [[2003.05339](#)].
- [30] J. F. Beacom, N. F. Bell and S. Dodelson, *Neutrinoless universe*, *Phys. Rev. Lett.* **93** (2004) 121302 [[astro-ph/0404585](#)].
- [31] Z. Chacko, L. J. Hall, T. Okui and S. J. Oliver, *CMB signals of neutrino mass generation*, *Phys. Rev. D* **70** (2004) 085008 [[hep-ph/0312267](#)].
- [32] Z. Chacko, L. J. Hall, S. J. Oliver and M. Perelstein, *Late time neutrino masses, the LSND experiment and the cosmic microwave background*, *Phys. Rev. Lett.* **94** (2005) 111801 [[hep-ph/0405067](#)].
- [33] S. Hannestad, *Structure formation with strongly interacting neutrinos - Implications for the cosmological neutrino mass bound*, *JCAP* **02** (2005) 011 [[astro-ph/0411475](#)].
- [34] S. Hannestad and G. Raffelt, *Constraining invisible neutrino decays with the cosmic microwave background*, *Phys. Rev. D* **72** (2005) 103514 [[hep-ph/0509278](#)].
- [35] N. F. Bell, E. Pierpaoli and K. Sigurdson, *Cosmological signatures of interacting neutrinos*, *Phys. Rev. D* **73** (2006) 063523 [[astro-ph/0511410](#)].
- [36] A. Friedland, K. M. Zurek and S. Bashinsky, *Constraining Models of Neutrino Mass and Neutrino Interactions with the Planck Satellite*, [0704.3271](#).
- [37] M. Archidiacono, S. Gariazzo, C. Giunti, S. Hannestad, R. Hansen, M. Laveder et al., *Pseudoscalar—sterile neutrino interactions: reconciling the cosmos with neutrino oscillations*, *JCAP* **08** (2016) 067 [[1606.07673](#)].
- [38] E. Di Valentino, C. Bøehm, E. Hivon and F. R. Bouchet, *Reducing the H_0 and σ_8 tensions with Dark Matter-neutrino interactions*, *Phys. Rev. D* **97** (2018) 043513 [[1710.02559](#)].
- [39] C. D. Kreisch, F.-Y. Cyr-Racine and O. Doré, *Neutrino puzzle: Anomalies, interactions, and cosmological tensions*, *Phys. Rev. D* **101** (2020) 123505 [[1902.00534](#)].
- [40] M. Park, C. D. Kreisch, J. Dunkley, B. Hadzhiyska and F.-Y. Cyr-Racine, *Λ CDM or self-interacting neutrinos: How CMB data can tell the two models apart*, *Phys. Rev. D* **100** (2019) 063524 [[1904.02625](#)].

- [41] F. Forastieri, M. Lattanzi and P. Natoli, *Cosmological constraints on neutrino self-interactions with a light mediator*, *Phys. Rev. D* **100** (2019) 103526 [[1904.07810](#)].
- [42] M. Escudero and S. J. Witte, *A CMB search for the neutrino mass mechanism and its relation to the Hubble tension*, *Eur. Phys. J. C* **80** (2020) 294 [[1909.04044](#)].
- [43] S. Ghosh, R. Khatri and T. S. Roy, *Dark Neutrino interactions phase out the Hubble tension*, *Phys. Rev. D* **102** (2020) 123544 [[1908.09843](#)].
- [44] A. Mazumdar, S. Mohanty and P. Parashari, *Flavour specific neutrino self-interaction: H_0 tension and IceCube*, [2011.13685](#).
- [45] S. Roy Choudhury, S. Hannestad and T. Tram, *Updated constraints on massive neutrino self-interactions from cosmology in light of the H_0 tension*, [2012.07519](#).
- [46] T. Brinckmann, J. H. Chang and M. LoVerde, *Self-interacting neutrinos, the Hubble parameter tension, and the Cosmic Microwave Background*, [2012.11830](#).
- [47] B. Dasgupta and J. Kopp, *Cosmologically Safe eV-Scale Sterile Neutrinos and Improved Dark Matter Structure*, *Phys. Rev. Lett.* **112** (2014) 031803 [[1310.6337](#)].
- [48] S. Hannestad, R. S. Hansen and T. Tram, *How Self-Interactions can Reconcile Sterile Neutrinos with Cosmology*, *Phys. Rev. Lett.* **112** (2014) 031802 [[1310.5926](#)].
- [49] X. Chu, B. Dasgupta and J. Kopp, *Sterile neutrinos with secret interactions—lasting friendship with cosmology*, *JCAP* **10** (2015) 011 [[1505.02795](#)].
- [50] J. F. Cherry, A. Friedland and I. M. Shoemaker, *Short-baseline neutrino oscillations, Planck, and IceCube*, [1605.06506](#).
- [51] F. Forastieri, M. Lattanzi, G. Mangano, A. Mirizzi, P. Natoli and N. Saviano, *Cosmic microwave background constraints on secret interactions among sterile neutrinos*, *JCAP* **07** (2017) 038 [[1704.00626](#)].
- [52] N. Song, M. Gonzalez-Garcia and J. Salvado, *Cosmological constraints with self-interacting sterile neutrinos*, *JCAP* **10** (2018) 055 [[1805.08218](#)].
- [53] X. Chu, B. Dasgupta, M. Dentler, J. Kopp and N. Saviano, *Sterile neutrinos with secret interactions—cosmological discord?*, *JCAP* **11** (2018) 049 [[1806.10629](#)].
- [54] M. Berbig, S. Jana and A. Trautner, *The Hubble tension and a renormalizable model of gauged neutrino self-interactions*, *Phys. Rev. D* **102** (2020) 115008 [[2004.13039](#)].
- [55] Y. Farzan, *A model for large non-standard interactions of neutrinos leading to the LMA-Dark solution*, *Phys. Lett. B* **748** (2015) 311 [[1505.06906](#)].
- [56] Y. Farzan and I. M. Shoemaker, *Lepton Flavor Violating Non-Standard Interactions via Light Mediators*, *JHEP* **07** (2016) 033 [[1512.09147](#)].
- [57] B. Pontecorvo, *Neutrino Experiments and the Problem of Conservation of Leptonic Charge*, *Sov. Phys. JETP* **26** (1968) 984.
- [58] V. Gribov and B. Pontecorvo, *Neutrino astronomy and lepton charge*, *Phys. Lett. B* **28** (1969) 493.
- [59] M. Gonzalez-Garcia and M. Maltoni, *Phenomenology with Massive Neutrinos*, *Phys. Rept.* **460** (2008) 1 [[0704.1800](#)].
- [60] EUCLID collaboration, *Euclid Definition Study Report*, [1110.3193](#).
- [61] J. Hamann, S. Hannestad and Y. Y. Wong, *Measuring neutrino masses with a future galaxy survey*, *JCAP* **11** (2012) 052 [[1209.1043](#)].
- [62] DESI collaboration, *The DESI Experiment Part I: Science, Targeting, and Survey Design*, [1611.00036](#).

- [63] T. Sprenger, M. Archidiacono, T. Brinckmann, S. Clesse and J. Lesgourgues, *Cosmology in the era of Euclid and the Square Kilometre Array*, *JCAP* **02** (2019) 047 [[1801.08331](#)].
- [64] KATRIN collaboration, *Improved Upper Limit on the Neutrino Mass from a Direct Kinematic Method by KATRIN*, *Phys. Rev. Lett.* **123** (2019) 221802 [[1909.06048](#)].
- [65] B. Monreal and J. A. Formaggio, *Relativistic Cyclotron Radiation Detection of Tritium Decay Electrons as a New Technique for Measuring the Neutrino Mass*, *Phys. Rev. D* **80** (2009) 051301 [[0904.2860](#)].
- [66] L. Gastaldo et al., *The Electron Capture ^{163}Ho Experiment ECHO: an overview*, *J. Low Temp. Phys.* **176** (2014) 876 [[1309.5214](#)].
- [67] B. Alpert et al., *HOLMES - The Electron Capture Decay of ^{163}Ho to Measure the Electron Neutrino Mass with sub-eV sensitivity*, *Eur. Phys. J. C* **75** (2015) 112 [[1412.5060](#)].
- [68] M. Croce et al., *Development of holmium-163 electron-capture spectroscopy with transition-edge sensors*, *J. Low Temp. Phys.* **184** (2016) 958 [[1510.03874](#)].
- [69] M. Gonzalez-Garcia, M. Maltoni and J. Salvado, *Robust Cosmological Bounds on Neutrinos and their Combination with Oscillation Results*, *JHEP* **08** (2010) 117 [[1006.3795](#)].
- [70] A. Cuoco, J. Lesgourgues, G. Mangano and S. Pastor, *Do observations prove that cosmological neutrinos are thermally distributed?*, *Phys. Rev. D* **71** (2005) 123501 [[astro-ph/0502465](#)].
- [71] I. M. Oldengott, G. Barenboim, S. Kahlen, J. Salvado and D. J. Schwarz, *How to relax the cosmological neutrino mass bound*, *JCAP* **04** (2019) 049 [[1901.04352](#)].
- [72] N. Bellomo, E. Bellini, B. Hu, R. Jimenez, C. Pena-Garay and L. Verde, *Hiding neutrino mass in modified gravity cosmologies*, *JCAP* **02** (2017) 043 [[1612.02598](#)].
- [73] S. Vagnozzi, E. Giusarma, O. Mena, K. Freese, M. Gerbino, S. Ho et al., *Unveiling ν secrets with cosmological data: neutrino masses and mass hierarchy*, *Phys. Rev. D* **96** (2017) 123503 [[1701.08172](#)].
- [74] S. Vagnozzi, S. Dhawan, M. Gerbino, K. Freese, A. Goobar and O. Mena, *Constraints on the sum of the neutrino masses in dynamical dark energy models with $w(z) \geq -1$ are tighter than those obtained in Λ CDM*, *Phys. Rev. D* **98** (2018) 083501 [[1801.08553](#)].
- [75] S. Gariazzo and O. Mena, *Cosmology-marginalized approaches in Bayesian model comparison: The neutrino mass as a case study*, *Phys. Rev. D* **99** (2019) 021301 [[1812.05449](#)].
- [76] Z. Chacko, A. Dev, P. Du, V. Poulin and Y. Tsai, *Cosmological Limits on the Neutrino Mass and Lifetime*, *JHEP* **04** (2020) 020 [[1909.05275](#)].
- [77] M. Escudero, J. Lopez-Pavon, N. Rius and S. Sandner, *Relaxing Cosmological Neutrino Mass Bounds with Unstable Neutrinos*, [2007.04994](#).
- [78] PLANCK collaboration, *Planck 2018 results. VI. Cosmological parameters*, *Astron. Astrophys.* **641** (2020) A6 [[1807.06209](#)].
- [79] R. Fardon, A. E. Nelson and N. Weiner, *Dark energy from mass varying neutrinos*, *JCAP* **10** (2004) 005 [[astro-ph/0309800](#)].
- [80] D. B. Kaplan, A. E. Nelson and N. Weiner, *Neutrino oscillations as a probe of dark energy*, *Phys. Rev. Lett.* **93** (2004) 091801 [[hep-ph/0401099](#)].
- [81] P. Gu, X. Wang and X. Zhang, *Dark energy and neutrino mass limits from baryogenesis*, *Phys. Rev. D* **68** (2003) 087301 [[hep-ph/0307148](#)].
- [82] R. Peccei, *Neutrino models of dark energy*, *Phys. Rev. D* **71** (2005) 023527 [[hep-ph/0411137](#)].
- [83] R. Bean and J. Magueijo, *Dilaton derived quintessence scenario leading naturally to the late time acceleration of the universe*, *Phys. Lett. B* **517** (2001) 177 [[astro-ph/0007199](#)].

- [84] C.-P. Ma and E. Bertschinger, *Cosmological perturbation theory in the synchronous and conformal Newtonian gauges*, *Astrophys. J.* **455** (1995) 7 [[astro-ph/9506072](#)].
- [85] K. Ichiki and Y.-Y. Keum, *Primordial Neutrinos, Cosmological Perturbations in Interacting Dark-Energy Model: CMB and LSS*, *JCAP* **06** (2008) 005 [[0705.2134](#)].
- [86] G. W. Anderson and S. M. Carroll, *Dark matter with time dependent mass*, in *1st International Conference on Particle Physics and the Early Universe*, pp. 227–229, 9, 1997, [astro-ph/9711288](#), DOI.
- [87] A. Friedman, *On the Curvature of space*, *Z. Phys.* **10** (1922) 377.
- [88] A. Friedmann, *On the Possibility of a world with constant negative curvature of space*, *Z. Phys.* **21** (1924) 326.
- [89] H. Robertson, *Kinematics and World-Structure*, *Astrophys. J.* **82** (1935) 284.
- [90] A. G. Walker, *On Milne’s Theory of World-Structure*, *Proceedings of the London Mathematical Society* **s2-42** (1937) 90 [<https://londmathsoc.onlinelibrary.wiley.com/doi/pdf/10.1112/plms/s2-42.1.90>].
- [91] B. Ratra and P. Peebles, *Cosmological Consequences of a Rolling Homogeneous Scalar Field*, *Phys. Rev. D* **37** (1988) 3406.
- [92] C. Wetterich, *Cosmology and the Fate of Dilatation Symmetry*, *Nucl. Phys. B* **302** (1988) 668 [[1711.03844](#)].
- [93] J. A. Frieman, C. T. Hill, A. Stebbins and I. Waga, *Cosmology with ultralight pseudo Nambu-Goldstone bosons*, *Phys. Rev. Lett.* **75** (1995) 2077 [[astro-ph/9505060](#)].
- [94] K. Coble, S. Dodelson and J. A. Frieman, *Dynamical Lambda models of structure formation*, *Phys. Rev. D* **55** (1997) 1851 [[astro-ph/9608122](#)].
- [95] R. Caldwell, R. Dave and P. J. Steinhardt, *Cosmological imprint of an energy component with general equation of state*, *Phys. Rev. Lett.* **80** (1998) 1582 [[astro-ph/9708069](#)].
- [96] E. J. Copeland, M. Sami and S. Tsujikawa, *Dynamics of dark energy*, *Int. J. Mod. Phys. D* **15** (2006) 1753 [[hep-th/0603057](#)].
- [97] S. Tsujikawa, *Quintessence: A Review*, *Class. Quant. Grav.* **30** (2013) 214003 [[1304.1961](#)].
- [98] G. D’Amico, T. Hamill and N. Kaloper, *Neutrino Masses from Outer Space*, *Phys. Lett. B* **797** (2019) 134846 [[1804.01542](#)].
- [99] N. Afshordi, M. Zaldarriaga and K. Kohri, *On the stability of dark energy with mass-varying neutrinos*, *Phys. Rev. D* **72** (2005) 065024 [[astro-ph/0506663](#)].
- [100] L. Beca and P. Avelino, *Dynamics of perfect fluid Unified Dark Energy models*, *Mon. Not. Roy. Astron. Soc.* **376** (2007) 1169 [[astro-ph/0507075](#)].
- [101] M. Kaplinghat and A. Rajaraman, *Stable models of super-acceleration*, *Phys. Rev. D* **75** (2007) 103504 [[astro-ph/0601517](#)].
- [102] O. E. Bjaelde, A. W. Brookfield, C. van de Bruck, S. Hannestad, D. F. Mota, L. Schremp et al., *Neutrino Dark Energy – Revisiting the Stability Issue*, *JCAP* **01** (2008) 026 [[0705.2018](#)].
- [103] R. Bean, E. E. Flanagan and M. Trodden, *The Adiabatic Instability on Cosmology’s Dark Side*, *New J. Phys.* **10** (2008) 033006 [[0709.1124](#)].
- [104] P. F. de Salas and S. Pastor, *Relic neutrino decoupling with flavour oscillations revisited*, *JCAP* **07** (2016) 051 [[1606.06986](#)].
- [105] K. Akita and M. Yamaguchi, *A precision calculation of relic neutrino decoupling*, *JCAP* **08** (2020) 012 [[2005.07047](#)].

- [106] J. Froustey, C. Pitrou and M. C. Volpe, *Neutrino decoupling including flavour oscillations and primordial nucleosynthesis*, *JCAP* **12** (2020) 015 [[2008.01074](#)].
- [107] J. J. Bennett, G. Buldgen, P. F. de Salas, M. Drewes, S. Gariazzo, S. Pastor et al., *Towards a precision calculation of N_{eff} in the Standard Model II: Neutrino decoupling in the presence of flavour oscillations and finite-temperature QED*, [2012.02726](#).
- [108] M. Escudero Abenza, *Precision early universe thermodynamics made simple: N_{eff} and neutrino decoupling in the Standard Model and beyond*, *JCAP* **05** (2020) 048 [[2001.04466](#)].
- [109] M. Escudero and M. Fairbairn, *Cosmological Constraints on Invisible Neutrino Decays Revisited*, *Phys. Rev. D* **100** (2019) 103531 [[1907.05425](#)].
- [110] V. Barger, P. Huber and D. Marfatia, *Solar mass-varying neutrino oscillations*, *Phys. Rev. Lett.* **95** (2005) 211802 [[hep-ph/0502196](#)].
- [111] M. Cirelli, M. Gonzalez-Garcia and C. Pena-Garay, *Mass varying neutrinos in the sun*, *Nucl. Phys. B* **719** (2005) 219 [[hep-ph/0503028](#)].
- [112] K. S. Babu, G. Chauhan and P. S. Bhupal Dev, *Neutrino nonstandard interactions via light scalars in the Earth, Sun, supernovae, and the early Universe*, *Phys. Rev. D* **101** (2020) 095029 [[1912.13488](#)].
- [113] F. Beutler, C. Blake, M. Colless, D. Jones, L. Staveley-Smith, L. Campbell et al., *The 6dF Galaxy Survey: Baryon Acoustic Oscillations and the Local Hubble Constant*, *Mon. Not. Roy. Astron. Soc.* **416** (2011) 3017 [[1106.3366](#)].
- [114] A. J. Ross, L. Samushia, C. Howlett, W. J. Percival, A. Burden and M. Manera, *The clustering of the SDSS DR7 main Galaxy sample – I. A 4 per cent distance measure at $z = 0.15$* , *Mon. Not. Roy. Astron. Soc.* **449** (2015) 835 [[1409.3242](#)].
- [115] BOSS collaboration, *The clustering of galaxies in the completed SDSS-III Baryon Oscillation Spectroscopic Survey: cosmological analysis of the DR12 galaxy sample*, *Mon. Not. Roy. Astron. Soc.* **470** (2017) 2617 [[1607.03155](#)].
- [116] B. Audren, J. Lesgourgues, S. Bird, M. G. Haehnelt and M. Viel, *Neutrino masses and cosmological parameters from a Euclid-like survey: Markov Chain Monte Carlo forecasts including theoretical errors*, *JCAP* **01** (2013) 026 [[1210.2194](#)].
- [117] J. Lesgourgues, *The Cosmic Linear Anisotropy Solving System (CLASS) I: Overview*, [1104.2932](#).
- [118] D. Blas, J. Lesgourgues and T. Tram, *The Cosmic Linear Anisotropy Solving System (CLASS) II: Approximation schemes*, *JCAP* **07** (2011) 034 [[1104.2933](#)].
- [119] J. Lesgourgues, *The Cosmic Linear Anisotropy Solving System (CLASS) III: Comparison with CAMB for LambdaCDM*, [1104.2934](#).
- [120] J. Lesgourgues and T. Tram, *The Cosmic Linear Anisotropy Solving System (CLASS) IV: efficient implementation of non-cold relics*, *JCAP* **09** (2011) 032 [[1104.2935](#)].
- [121] B. Audren, J. Lesgourgues, K. Benabed and S. Prunet, *Conservative Constraints on Early Cosmology: an illustration of the Monte Python cosmological parameter inference code*, *JCAP* **1302** (2013) 001 [[1210.7183](#)].
- [122] T. Brinckmann and J. Lesgourgues, *MontePython 3: boosted MCMC sampler and other features*, [1804.07261](#).
- [123] A. Gelman and D. B. Rubin, *Inference from Iterative Simulation Using Multiple Sequences*, *Statist. Sci.* **7** (1992) 457.
- [124] I. Esteban, M. Gonzalez-Garcia, M. Maltoni, T. Schwetz and A. Zhou, *The fate of hints: updated global analysis of three-flavor neutrino oscillations*, *JHEP* **09** (2020) 178 [[2007.14792](#)]. NuFIT 5.0 (2020), [www.nu-fit.org](#).

- [125] P. de Salas, D. Forero, S. Gariazzo, P. Martínez-Miravé, O. Mena, C. Ternes et al., *2020 Global reassessment of the neutrino oscillation picture*, [2006.11237](#).
- [126] F. Capozzi, E. Di Valentino, E. Lisi, A. Marrone, A. Melchiorri and A. Palazzo, *Global constraints on absolute neutrino masses and their ordering*, *Phys. Rev. D* **95** (2017) 096014 [[2003.08511](#)]. [Addendum: *Phys.Rev.D* 101, 116013 (2020)].
- [127] J. Lesgourgues, G. Mangano, G. Miele and S. Pastor, *Neutrino Cosmology*. Cambridge University Press, 2, 2013.
- [128] DES collaboration, *Dark Energy Survey year 1 results: Cosmological constraints from galaxy clustering and weak lensing*, *Phys. Rev. D* **98** (2018) 043526 [[1708.01530](#)].
- [129] DES collaboration, *Dark Energy Survey Year 1 results: Cosmological constraints from cosmic shear*, *Phys. Rev. D* **98** (2018) 043528 [[1708.01538](#)].
- [130] KiDS collaboration, *KiDS-1000 Cosmology: Cosmic shear constraints and comparison between two point statistics*, *Astron. Astrophys.* **645** (2021) A104 [[2007.15633](#)].
- [131] HSC collaboration, *Cosmology from cosmic shear power spectra with Subaru Hyper Suprime-Cam first-year data*, *Publ. Astron. Soc. Jap.* **71** (2019) Publications of the Astronomical Society of Japan, Volume 71, Issue 2, April 2019, 43, <https://doi.org/10.1093/pasj/psz010> [[1809.09148](#)].
- [132] SKA COSMOLOGY SWG collaboration, *Overview of Cosmology with the SKA*, *PoS AASKA14* (2015) 016 [[1501.04076](#)].
- [133] LSST DARK ENERGY SCIENCE collaboration, *The LSST Dark Energy Science Collaboration (DESC) Science Requirements Document*, [1809.01669](#).
- [134] L. Verde, T. Treu and A. Riess, *Tensions between the Early and the Late Universe*, *Nature Astron.* **3** (2019) 891 [[1907.10625](#)].
- [135] R. Takahashi, M. Sato, T. Nishimichi, A. Taruya and M. Oguri, *Revising the Halofit Model for the Nonlinear Matter Power Spectrum*, *Astrophys. J.* **761** (2012) 152 [[1208.2701](#)].
- [136] S. Bird, M. Viel and M. G. Haehnelt, *Massive Neutrinos and the Non-linear Matter Power Spectrum*, *Mon. Not. Roy. Astron. Soc.* **420** (2012) 2551 [[1109.4416](#)].
- [137] E. Castorina, E. Sefusatti, R. K. Sheth, F. Villaescusa-Navarro and M. Viel, *Cosmology with massive neutrinos II: on the universality of the halo mass function and bias*, *JCAP* **02** (2014) 049 [[1311.1212](#)].
- [138] E. Castorina, C. Carbone, J. Bel, E. Sefusatti and K. Dolag, *DEMNUi: The clustering of large-scale structures in the presence of massive neutrinos*, *JCAP* **07** (2015) 043 [[1505.07148](#)].
- [139] S. Vagnozzi, T. Brinckmann, M. Archidiacono, K. Freese, M. Gerbino, J. Lesgourgues et al., *Bias due to neutrinos must not uncorrect'd go*, *JCAP* **09** (2018) 001 [[1807.04672](#)].
- [140] A. Raccanelli, L. Verde and F. Villaescusa-Navarro, *Biases from neutrino bias: to worry or not to worry?*, *Mon. Not. Roy. Astron. Soc.* **483** (2019) 734 [[1704.07837](#)].
- [141] E. Sudarshan, *Equivalence of semiclassical and quantum mechanical descriptions of statistical light beams*, *Phys. Rev. Lett.* **10** (1963) 277.
- [142] R. J. Glauber, *Coherent and incoherent states of the radiation field*, *Phys. Rev.* **131** (1963) 2766.
- [143] R. J. Glauber, *The Quantum theory of optical coherence*, *Phys. Rev.* **130** (1963) 2529.
- [144] M. E. Peskin and D. V. Schroeder, *An Introduction to quantum field theory*. Addison-Wesley, Reading, USA, 1995.